NDARC — NASA Design and Analysis of Rotorcraft Validation and Demonstration

Wayne Johnson
Aeromechanics Branch
National Aeronautics and Space Administration
Ames Research Center, Moffett Field, California
wayne.johnson@nasa.gov

ABSTRACT

Validation and demonstration results from the development of the conceptual design tool NDARC (NASA Design and Analysis of Rotorcraft) are presented. The principal tasks of NDARC are to design a rotorcraft to satisfy specified design conditions and missions, and then analyze the performance of the aircraft for a set of off-design missions and point operating conditions. The aircraft chosen as NDARC development test cases are the UH-60A single main-rotor and tail-rotor helicopter, the CH-47D tandem helicopter, the XH-59A coaxial lift-offset helicopter, and the XV-15 tiltrotor. These aircraft were selected because flight performance data, a weight statement, detailed geometry information, and a correlated comprehensive analysis model are available for each. Validation consists of developing the NDARC models for these aircraft by using geometry and weight information, airframe wind tunnel test data, engine decks, rotor performance tests, and comprehensive analysis results; and then comparing the NDARC results for aircraft and component performance with flight test data. Based on the calibrated models, the capability of the code to size rotorcraft is explored.

INTRODUCTION*

The objectives of rotorcraft design work in a government laboratory are to support research and to support rotorcraft acquisition. Research activities require a robust design capability to aid in technology impact assessments and to provide system level context for research. At the applied research level, it is necessary to show how technology will impact future systems, and justify the levels of investment required to mature that technology to an engineering development stage. Design provides one avenue to accomplishing these objectives. The Department of Defense (DoD) acquisition phases requiring rotorcraft design work include concept exploration, concept decision, concept refinement, and technology development. During these acquisition phases, it is typically necessary to perform quantitative evaluation and independent synthesis of a wide array of aircraft designs, in order to provide the foundation for specification and requirement development.

Rotorcraft conceptual design consists of analysis, synthesis, and optimization to find the best aircraft meeting the required capabilities and performance. A conceptual design tool is used for synthesis and analysis of rotorcraft. These tools historically have been low fidelity for rapid application. Such sizing codes are built around the use of momentum theory for rotors, classical finite wing theory, a referred parameter engine model, and semi-empirical weight estimation techniques. The successful use of a low-fidelity tool requires careful consideration of model input parameters and judicious comparison with existing aircraft to avoid unjustified extrapolation of results.

The helicopter industry has proprietary conceptual design tools, including PRESTO (Bell Helicopter), RDM (Sikorsky Aircraft), and HESCOMP and VASCOMP (Boeing). Until now the tools available to the U.S. government have been characterized by out-of-date

*Presented at the American Helicopter Society Aeromechanics Specialists' Conference, San Francisco, CA, January 20-22, 2010.

software and limited capabilities. Examples are HESCOMP and VASCOMP (the versions developed by Boeing in the 1970s), and RC (developed by the U.S. Army AFDD in the 1990s).

NASA, with support from the U.S. Army, conducted in 2005 the NASA Heavy Lift Rotorcraft Systems Investigation (ref. 1), focused on the design and in-depth analysis of rotorcraft configurations that could satisfy the Vehicle Systems Program (VSP) technology goals. The VSP technology goals and mission were intended to identify enabling technology for civil application of heavy lift rotorcraft. The goals emphasized efficient cruise and hover, efficient structure, and low noise. The requirements included carrying 120 passengers over a 1200 nm range, 350 knots at 30,000 ft altitude. The configurations considered included the Large Civil Tiltrotor (LCTR), Large Civil Tandem Compound (LCTC), and Large Advancing Blade Concept (LABC). This project is an example of the role of a rotorcraft sizing code within a government laboratory. The design tool used was the AFDD RC code. The project illustrated the difficulties adapting or modifying a legacy code for configurations other than conventional helicopters and tiltrotors.

Since 2005, there have been numerous other joint NASA/U.S. Army investigations of advanced rotorcraft concepts, covering conventional tiltrotors and helicopters, slowed-rotor compound helicopters (ref. 2), a tilting-tandem concept, heavy-lift slowed-rotor tiltrotors (ref. 3), lift-offset rotor concepts (ref. 4), and a second generation large civil tiltrotor (LCTR2, ref. 5). These design projects have gone well beyond the conventional boundaries of the conceptual design process, combining high-fidelity analyses (including rotorcraft comprehensive analysis, computational fluid dynamics, and structural analysis) with the conceptual design tool. This approach has been required because of the increasing sophistication of the requirements and the technology, and the increased level of certainty needed to differentiate between system concepts.

Based on this experience, a new conceptual design tool has been developed to support future needs of the NASA Subsonic Rotary Wing project and the U.S. Army AFDD Advanced Design Office: NASA Design and Analysis of Rotorcraft (NDARC). The software development started in January 2007, and the initial code release occurred in May 2009. This paper presents validation and demonstration results from the NDARC development. A companion paper (ref. 6) summarizes the NDARC theoretical basis and architecture; the complete description is in reference 7.

Validation consists of developing the NDARC models for an aircraft by using geometry and weight information, airframe wind tunnel test data, engine decks, rotor tests, and comprehensive analysis results; and then comparing the NDARC results for aircraft and component performance with flight test data. The validation process is illustrated in Figure 1. Based on the calibrated models, the capability of the code to size rotorcraft is explored.

DEVELOPMENT TEST CASES

The aircraft chosen for NDARC development test cases are the UH-60A single main-rotor and tail-rotor helicopter, the CH-47D tandem helicopter, the XH-59A coaxial lift-offset helicopter, and the XV-15 tiltrotor (figure 2). These aircraft were selected because flight performance data, a weight statement, detailed geometry information, and a correlated comprehensive analysis model are available for each. Table 1 presents the principal characteristics of the four aircraft. The aircraft are described in references 8 to 16. Figure 3 illustrates the NDARC models.

Rotor Performance Model

The NDARC rotor performance model represents the rotor power as the sum of induced, profile, and parasite terms: $P = P_i + P_o + P_p$. The parasite power (including climb/descent power for the aircraft) is obtained from the wind axis drag force and rotor velocity: $P_p = -XV$. The induced power is calculated from the ideal power and the induced power factor κ: $P_i = \kappa P_{\text{ideal}}$. The profile power is calculated from a mean blade drag coefficient $c_{d\,\text{mean}}$: $C_{Po} = (\sigma/8) c_{d\,\text{mean}} F_P$, where the function $F_P(\mu, \mu_z)$ accounts for the increase of the blade section velocity with rotor edgewise and axial speed. The induced and profile power can not be measured separately in a wind tunnel or flight test, only the sum is available from $P_i + P_o = P + XV$ (if the rotor wind-axis drag force X is measured or estimated). Therefore analysis is used to separate induced and profile power. The steps in the approach are: first correlate performance calculations from a comprehensive analysis with wind tunnel or flight test data; next develop the parameters of the NDARC rotor performance model based on calculated κ and $c_{d\,\text{mean}}$ for the appropriate range of flight conditions; and finally compare the NDARC performance calculations with the test data. The rotorcraft comprehensive analysis used for the present effort is CAMRADII (refs. 17 and 18).

Interference from Rotors

The aerodynamic interference of the rotors on the airframe (fuselage, tail, and wing) is required to calculate the hover download. The default model (refs. 6 and 7) has a very fast rate of development, such that the induced velocity quickly attains a value equal to the fully developed wake velocity. This is based on tests that show the drag of bodies immersed in the wake varies little with distance below the rotor disk, the time variation of the wake-induced velocity decreasing as the magnitude of the mean velocity increases with distance. The transition from inside to outside the wake boundary takes place over a finite-width wake boundary; the default width is 0.2 times the contracted radius. The default interference factor is $K_{\text{int}} = 1.0$ for each component. The vertical drag values are set to give the known hover download.

Engines

The parameters that describe the T700-GE-700 engine (for UH-60A) and T55-L-712 engine (for CH-47D) in the Referred Parameter Turboshaft Engine Model (RPTEM) were developed by AFDD, using data obtained by running engine decks. The RPTEM description of the LTC1K-4K engine (modified T53-L-13B, for XV-15) was based on parameters for a generic 2000 hp engine, the power and specific fuel consumption at four ratings, and jet thrust data. The description of the PT6T-3 engine (for XH-59A) was based on parameters for a generic 2000 hp engine, and the power and specific fuel consumption at two ratings. References 6 and 7 provide details of the RPTEM model. Information obtained from engine decks is usually proprietary, so no further information is presented here.

Weights

Using the known aircraft parameters, weights of the components were estimated using the parametric models described in references 6 and 7. The actual weights are available from February 1988 (MIL-STD-1374) for the UH-60A; from September 1985 (MIL-STD-451) for the CH-47D; from May 1972 and March 1978 (MIL-STD-451) for the XH-59A helicopter configuration, including compound increments; and from February 1977 (MIL-STD-451) for the XV-15. The ratio of the actual weight to the parametric weight is a calibration factor. By using calibration factors, the NDARC weight statement matches the actual aircraft weight statement. In the context of a new aircraft design, these factors account for the impact of technology.

The derived calibration factors are presented in table 2. Note that the tiltrotor wing model was calibrated for the XV-15, and the lift-offset rotor weight model was calibrated for the XH-59A (ref. 7), so the corresponding calibration factors are nearly unity. With some exceptions, the calibration factors are within the error range of the parametric equations (ref. 7). The errors of the equations estimating the horizontal tail and vertical tail weights are greater than 20%, but the error is even larger for the vertical tail in these examples. The higher weight of the XV-15 horizontal tail might be attributable to the H-tail configuration. The error of the equation estimating the accessory weight is about 11%; the error is larger for all aircraft here. The calibration factors for the landing gear and the engine support of the UH-60A presumably reflect design approach. The calibration factors for the CH-47D and XH-59A flight controls, and the XH-59A engine support, may reflect the rotorcraft configuration. The calibration factors for the XV-15 engine cowling and fuel system may be due to the experimental character of the aircraft. The large calibration factor for the XV-15 drive system is a result of the tiltrotor configuration and the experimental character of the aircraft.

VALIDATION AND DEMONSTRATION RESULTS

UH-60A Helicopter

The NDARC model of the UH-60A single main-rotor and tail rotor helicopter is illustrated in figure 3. Table 1 presents the principal aircraft parameters.

The airframe aerodynamic model was developed based on quarter-scale wind tunnel test data, for tail-off and tail-on configurations. The model for lift, drag, and pitch moment shows good correlation with the wind tunnel data over the angle-of-attack range –30 to +30 deg, including the break in lift and moment slope where stall of the tail occurs. The model for side force shows good correlation with the wind tunnel data over the sideslip angle range –30 to +30 deg. The model for roll moment and pitch moment shows only fair correlation, over the sideslip angle range –10 to +10 deg. The results are not shown here since the wind tunnel data are not publically available.

The UH-60A Airloads flight test (ref. 19) provides measurements of the aircraft, main rotor, and tail rotor power for a range of blade loading and advance ratio. Correlation of CAMRADII performance calculations with these flight test data was presented in reference 20, along with discussion of the power losses and aircraft drag. The aircraft drag was adjusted to match the Airloads flight test configuration, and the horizontal tail incidence was set to the measured value. Figure 4 shows the CAMRADII performance correlation.

Figures 5 to 10 compare the NDARC UH-60A model with the CAMRADII calculations of the induced power factor κ and mean drag coefficient $c_{d\,\mathrm{mean}}$. The model parameters were adjusted to obtain the correlation shown. Table 3 gives the parameters used. The equations of the NDARC model accommodate the variation of κ and $c_{d\,\mathrm{mean}}$ with blade loading C_T/σ in hover (figures 5 and 7); the increase of κ with advance ratio μ in forward flight (figure 6); and the increase of $c_{d\,\mathrm{mean}}$ with advancing tip Mach number M_{at} in forward flight (figure 8). The profile power stall loading $(C_T/\sigma)_s$ and its decrease with μ (figure 9) is responsible for the increase of $c_{d\,\mathrm{mean}}$ with C_T/σ and μ (figure 10).

A similar process was followed to develop the NDARC UH-60A tail rotor performance model. The CAMRADII calculations used momentum theory for the induced power. The profile power results are shown in figures 11 to 13. Figure 14 compares the NDARC calculation of the tail rotor hover power with whirl test measurements (ref. 21).

Flight test hover performance (refs. 22 and 23) is compared with NDARC calculations in figure 15. Correlation of the NDARC performance calculations with the UH-60A Airloads flight test data is shown in figure 16. The NDARC performance model of the UH-60A helicopter gives generally good results. At high C_T/σ the tail rotor power is larger than measured, likely reflecting differences in trim.

Table 4 shows the helicopter design missions and flight conditions considered here. These criteria are based on the UTTAS system specification (ref. 24). Based on the calibrated UH-60A performance and engine models, the NDARC calculations of the helicopter capability are as follows.

Flight conditions:
a) OGE hover vertical rate-of-climb: 584 ft/min
b) Maximum cruise speed: 145 knots
c) Maximum alternate gross weight: 20914 lb
d) OEI level flight speed: 107 knots
d) OEI service ceiling: 5136 ft
e) OEI hover IGE: 14330 lb gross weight

Missions:
f) Primary mission: 121 minutes endurance, or 16777 lb gross weight, or 139 nm range
g) Fuel tank design: 151 minutes endurance, or 2751 lb fuel, or 192 nm range
h) Alternate endurance: 120 minutes endurance, or 17710 lb gross weight, or 131 nm range

To explore the sizing capability of NDARC, helicopters were designed to meet the criteria of table 4. Two sizing approaches are considered: size the rotor for fixed engine power, and size the engine for fixed disk loading. For each approach the technology factors were set either to the calibration values, or to unity. The blade loading C_W/σ, tip speed V_{tip}, and number of blades were held constant for both main rotor and tail rotor. The empennage tail volume and aspect ratio were held constant. Cost was estimated using technology factors equal 1.0. Table 5 summarizes the results of this demonstration of the NDARC sizing capability.

CH-47D Tandem Helicopter

The NDARC model of the CH-47D tandem helicopter is illustrated in figure 3. Table 1 presents the principal aircraft parameters.

Flight test measurements of CH-47D hover and forward flight performance are given in reference 11, including an estimate of aircraft power losses. The forward flight data includes variations of gross weight, altitude, and rotor tip speed. The aircraft drag was adjusted to match the flight test configuration. The airframe vertical drag was determined for the nominal hover download, then the rotor-to-fuselage interference factor was set to $K_{\mathrm{int}} = 0.73$ in order to get the required download with the tandem rotor interference model. Figure 17 shows the CAMRADII hover performance correlation, for a single rotor on a whirl stand, and for the aircraft in flight. Figure 18 shows the CAMRADII performance correlation for forward flight. Note that the power is under-predicted at high thrust.

Figures 19 to 26 compare the NDARC CH-47D model with the CAMRADII calculations of the induced power factor κ and mean drag coefficient $c_{d\,\mathrm{mean}}$. The model parameters were adjusted to obtain the correlation shown. Table 3 gives the parameters used. The equations of the NDARC model accommodate the variation of κ and $c_{d\,\mathrm{mean}}$ with blade loading C_T/σ in hover (figures 19 and 23, respectively); the increase of κ with advance ratio μ in forward flight (figure 20); and the increase of $c_{d\,\mathrm{mean}}$ with advancing tip Mach number M_{at} in forward flight (figure 24). The profile power stall loading $(C_T/\sigma)_s$ and its decrease with μ (figure 25) is responsible for the increase of $c_{d\,\mathrm{mean}}$ with C_T/σ and μ (figure 26).

The NDARC model can fit the induced power factor variation for a single rotor in hover and cruise well (figures 19 and 20). However, adjustments (simpler variation of hover factor with C_T/σ, less increase of forward flight factor with μ) are required to model the induced power of the tandem rotors. Figures 21 and 22 show the resulting fit of the NDARC model to the CAMRADII calculations of the aircraft (tandem rotor) induced power. The NDARC model can fit the mean drag coefficient for a single rotor in forward flight well (figure 26a), using the stall inception curve shown in figure 25 and the coefficients $d_{s1}=2$ and $d_{s2}=40$ (comparable to the UH-60A values). However, the CAMRADII calculations under-predict the power at high thrust (figure 18). Thus a better match to the flight test data is obtained by increasing the stall profile power (figure 26b), accomplished by increasing $(C_T/\sigma)_s$ at low speed and using $d_{s1}=4$ and $d_{s2}=120$ (table 3b).

Flight test hover performance is compared with NDARC calculations in figure 27. Correlation of the NDARC forward flight performance calculations with the CH-47D flight test data is shown in figure 28. The NDARC performance model of the CH-47D tandem helicopter gives generally good results. In particular, the power is predicted well in forward flight at high thrust.

Based on the calibrated CH-47D performance and engine models, the NDARC calculations of the helicopter capability are as follows. All conditions are at design gross weight, 4000 ft altitude, 95 deg F temperature unless noted.

a) Hover vertical rate of climb, 100% MRP: 707 ft/min
b) Maximum cruise speed, 100% MCP: 151 knots
c) Maximum takeoff weight, 100% MRP: 44055 lb
d) Maximum takeoff weight at SLS, 100% MRP: 54382 lb
e) Maximum takeoff weight at 10k/ISA, 100% MRP: 43973 lb
f) Service ceiling at ISA, 100% MCP: 21965 ft (80 knots)
g) Endurance for takeoff at DGW, 5000 lb payload, 30 minutes fuel reserve: 88 minutes ($V_{be}=82-80$ knots)
h) Endurance for takeoff at DGW, maximum fuel (payload 2039 lb), 30 minutes fuel reserve: 188 minutes ($V_{be}=83-76$ knots)

Table 6 shows the mission used to evaluate endurance.

XH-59A Coaxial Helicopter

The NDARC model of the XH-59A coaxial lift-offset helicopter is illustrated in figure 3. Table 1 presents the principal aircraft parameters.

Flight test measurements of XH-59A performance are given in reference 25 for hover and in reference 13 for forward flight. The aircraft aerodynamic model, including drag, was obtained from reference 12. The forward flight data includes operation as a helicopter and with auxiliary propulsion. The compound configuration had a design gross weight of 13000 lb. Figure 29 shows the CAMRADII hover performance correlation. Figures 30 and 31 show the CAMRADII performance correlation in forward flight, for helicopter operation and with auxiliary propulsion respectively. The helicopter mode results (figure 30) are for two gross weights (referred to SLS conditions), and two control system phase angles. The flight tests with auxiliary propulsion were conducted at gross weights from 11900 to 13300 lb; the calculated rotor L/D_e values for 11900 lb (shown in figure 31) and 13300 lb are similar. Lift offset (rotor roll moment divided by thrust times radius) in the range of 0.2 to 0.3 gives good results for the calculated efficiency of the compound configuration at high speed.

Figures 32 to 39 compare the NDARC XH-59A model with the CAMRADII calculations of the induced power factor κ and mean drag coefficient $c_{d\,\mathrm{mean}}$. The model parameters were adjusted to obtain the correlation shown. Table 3 gives the parameters used. The equations of the NDARC model accommodate the variation of κ and $c_{d\,\mathrm{mean}}$ with blade loading C_T/σ in hover (figures 32 and 35); the increase of κ with advance ratio μ in forward flight (figures 33 and 34, including the influence of lift offset); and the increase of $c_{d\,\mathrm{mean}}$ with advancing tip Mach number M_{at} in forward flight (figure 36). The profile power stall loading $(C_T/\sigma)_s$ and its decrease with μ (figure 37) is responsible for the increase of $c_{d\,\mathrm{mean}}$ with C_T/σ and μ (figures 38 and 39).

The NDARC model can fit the mean drag coefficient for a single rotor in forward flight well (figures 38a and 39a), using parameters $d_0=0.0098$, $d_{s1}=2$, $d_{s2}=150$, and $d_{m1}=.005$. However, a better match to the flight test data is obtained by increasing the stall profile power, by using $d_0=0.0105$, $d_{s1}=12$, $d_{s2}=40$, and $d_{m1}=.015$ (table 3b). The resulting variation in $c_{d\,\mathrm{mean}}$ is shown in figures 38b and 39b.

Flight test hover performance is compared with NDARC calculations in figure 40. Correlation of the NDARC performance calculations with the XH-59A flight test data is shown in figures 41 and 42, for helicopter operation and with auxiliary propulsion respectively. The NDARC performance model of the XH-59A coaxial helicopter gives generally good results.

XV-15 Tiltrotor

The NDARC model of the XV-15 tiltrotor is illustrated in figure 3. Table 1 presents the principal aircraft parameters.

Hover measurements of the XV-15 isolated rotor performance are given in reference 26. Flight test measurements of XV-15 aircraft hover and forward flight performance are given in reference 27. Figure 43 shows the CAMRADII hover performance correlation for the isolated XV-15 rotor. The CAMRADII calculations of the XV-15 rotor cruise performance (propeller operation) were based on the models developed using wind tunnel measurements of the JVX rotor performance (ref. 28).

The airframe aerodynamic model was developed using results from a real-time simulation model, which was based on wind tunnel test data. The NDARC models fit well the lift, drag, and pitch moment as a function of angle-of-attack, for several flap deflections and nacelle angles; including elevator and aileron derivatives. A good fit was also achieved for the side force as a function of sideslip angle and rudder deflection. The results are not shown here since the simulation model data are not publically available.

Figure 44 compares the NDARC calculation of the hover download with flight test measurements (ref. 27). The measured download was deduced by combining the flight test measurement of aircraft weight and rotor power, and the isolated rotor measurements of rotor thrust and power. The calculated download is based on the rotor interference velocities at the wing, since the fuselage fountain effect is not modeled. The download for zero flap angle is obtained using a wing drag coefficient of $c_{d90} = 1.48$, with a factor $K_{\text{int}} = 2.0$ on the interference velocity to compensate for the absence of download on the fuselage. The wing download model produces a variation with flap angle by accounting for the reduction in projected area as the flap angle increases. However, the reduction of download at 60 deg flap deflection is larger than can be attributed to the projected area change (the XV-15 inboard flap and flaperon area is 18.5% of the wing area).The area change was increased by a factor of 4.6 in order to produce the variation shown in figure 44.

The NDARC model of the LTC1K-4K engine jet thrust is compared with data from reference 27 in figure 45.

Figures 46 to 57 compare the NDARC XV-15 model with the CAMRADII calculations of the induced power factor κ and mean drag coefficient $c_{d\,\text{mean}}$. The model parameters were adjusted to obtain the correlation shown. Table 3 gives the parameters used. The equations of the NDARC model accommodate the variation of κ and $c_{d\,\text{mean}}$ with blade loading C_T/σ in hover, both in hover (figures 46 and 51) and in cruise (figures 47 and 52). The exception is the induced power in cruise at low thrust (figure 47), but the propulsive efficiency in cruise depends principally on the profile power. Figure 57 shows the variation of the cruise induced and profile power with nacelle angle-of-attack (zero deg for axial flow). The NDARC model does not have a significant variation with shaft angle-of-attack at high axial advance ratio, but at least the variations of induced and profile power will cancel to some extent in the total.

The equations of NDARC model performance in helicopter mode flight (nacelle angle 90 deg) reasonably well: the increase of κ with advance ratio μ in forward flight (figure 48), and the increase of $c_{d\,\text{mean}}$ with C_T/σ and μ (figure 54). Figure 53 shows the profile power stall loading $(C_T/\sigma)_s$. The equations model well the profile power in conversion (nacelle angles 60 and 30 deg) and airplane (nacelle angle 0 deg) mode flight (figures 55 and 56), but the representation of the induced power (figures 49 and 50) is less satisfactory. However, the performance characteristics most important in design and mission analysis are the hover profile and induced power, and the cruise profile power.

Isolated XV-15 rotor hover performance is compared with NDARC calculations in figure 58. Correlation of the NDARC performance calculations with the XV-15 flight test data is shown in figures 59 and 60. The NDARC performance model of the XV-15 tiltrotor gives generally good results.

To explore the sizing capability of NDARC, tiltrotors were designed to meet the criteria of table 7, varying the rotor cruise tip speed. The design criteria (table 7) are based on the capabilities of the XV-15 experimental aircraft. The engine was sized for a fixed hover tip speed of $V_{\text{tip}} = 740$ ft/sec, with cruise tip speed varied from $V_{\text{tip}} = 740$ to $V_{\text{tip}} = 450$ ft/sec. The technology factors were set to the calibration values. The rotor disk loading, blade loading C_W/σ, and tip speed V_{tip} were held constant. The wing loading and the wing-fuselage clearance were held constant. Table 8 presents the results, and figure 61 shows the variation of the principal size and efficiency parameters. The performance values shown are for the cruise segment of the design mission. The rotor cruise propulsive efficiency and the engine specific fuel consumption steadily increase as the design cruise tip speed decreases. The design aircraft size starts to increase at about $V_{\text{tip}} = 575$ ft/sec, primarily because above that value the engine power is determined by the hover ceiling requirement, while below that value the engine power is determined by the maximum speed requirement.

ASSESSMENT OF MODELS

Interference from Rotors

The default rotor interference model is used for all aircraft considered here, with the following adjustments. For the UH-60A, the tail rotor interference is turned off to avoid excessive interference at the vertical tail in low speed flight. The UH-60A horizontal tail incidence is scheduled with speed, so the rotor interference is active in forward flight. For the other aircraft, the interference was transitioned to zero in forward flight, to avoid unrealistic variations of attitude and power at low speed. For the CH-47D the transition speed was 5–20 knots (responsible for the kinks in the power curve at low speed in figure 28). For the XH-59A and XV-15, the transition speed was 5–10 knots. For the CH-47D, an interference factor of $K_{\text{int}} = 0.73$ was used for the fuselage. For the XV-15, an interference factor of $K_{\text{int}} = 2.0$ was used for the wing, with a wake boundary of 0.1 times the contracted radius. Thus an improved interference model is needed, one that can better represent the rotor-to-aircraft interference in low speed flight.

Download

The hover download is calculated based on the rotor wake-induced interference velocity at the airframe (fuselage, tail, and wing), and vertical drag areas of the components. This model gives good results for the helicopter configurations. For the tiltrotor configuration however, the absence of the fuselage fountain effect in the model and the calculation of the effect of flap deflection based on the wing projected area reduction are significant limitations, requiring compensation using empirical parameters (as described above for the XV-15). Thus an improved tiltrotor download model is needed.

Rotor Performance Model

The parameters developed for the NDARC rotor performance models are given in table 3. The equations of the NDARC models for rotor induced power factor κ and mean drag coefficient $c_{d\,\text{mean}}$ provided a good representation of the characteristics of the UH-60A, CH-47D, and XH-59A rotors. For these aircraft, the most significant issues were the differences between single rotor and twin rotor performance, and the differences between comprehensive analysis calculations and flight test measurements of performance. Operation of the XV-15 tiltrotor introduces additional dimensions of large axial flow and nacelle angle variation from 90 deg (helicopter) to 0 deg (airplane), and consequently the fit of the NDARC models is less successful. In particular, the representation of the induced power in cruise at low thrust and in conversion mode flight is not good. Also, the models do not accommodate the variation of induced and profile power with nacelle angle at high axial advance ratio. Thus an improved model of the rotor induced and profile power is needed, for a better representation of the complete range of operation encountered by tiltrotors.

FUTURE NDARC DEVELOPMENT

Description and analysis of conventional rotorcraft configurations is facilitated in NDARC, specifically the single main rotor and tail rotor helicopter, tandem helicopter, coaxial helicopter, and tiltrotor configurations. Novel and advanced concepts typically are modeled by starting with one of these conventional configurations. For example, compound rotorcraft can be constructed by adding wings and propellers. Modeling compound helicopter, quad tiltrotor, and autogyro configurations with NDARC requires developing default input, including aircraft control and trim strategies; and testing and validation. Accurate modeling of the tiltwing configuration requires development of a rotor-wing interference model to account for the aerodynamics of transition mode flight. Modeling the Gyrodyne configuration requires a reaction drive model.

The following models, capabilities, and features (not presented in order of priority) can be added to NDARC. A collaborative development of NDARC capabilities is anticipated.

a) Reaction drive, including control, internal aerodynamics and power, and engine model. It will be necessary to extend the definition of a propulsion group, beyond connecting rotors and engine groups by a drive train.
b) Stopped rotors.
c) Vectored wake and thrust of rotors.
d) Turbojet/turbofan engine model, piston engine model.
e) Rotor trailing edge flap control.
f) Flow control for fuselage and rotor.
g) Combined blade element/momentum theory for inflow (hover, axial, edgewise). Dynamic wake.
h) Rotor airfoil tables.
i) Ducted fan aerodynamic loads.
j) Compressible airframe aerodynamics.
k) Influence of rotor interference on wing induced drag.
l) Expanded vertical/short takeoff and landing calculation

capability in mission analysis, including optimal control.
m) V-tail model (requiring two aerodynamic collocation points).
n) Aircraft center-of-gravity and moments of inertia (requires distribution of the weight of payload, fuel, and other components).
o) Engine and rotor noise estimation, based on empirical models.
p) Improved cost model, including engine costs and DOC model.
q) Improved models for rotor induced and profile power: in particular, tiltrotor model, effect of lift and propulsive force, effect of rotor parameters.

CONCLUDING REMARKS

Validation and demonstration results from the development of the conceptual design tool NDARC (NASA Design and Analysis of Rotorcraft) have been presented. The principal tasks of NDARC are to design a rotorcraft to satisfy specified design conditions and missions, and then analyze the performance of the aircraft for a set of off-design missions and point operating conditions.

The validation process involves developing the NDARC models for an aircraft by using geometry and weight information, airframe wind tunnel test data, engine decks, rotor performance tests, and comprehensive analysis results. Comprehensive analysis calculations are required in order to develop separate rotor induced power and profile power models. Then NDARC results for aircraft and component performance are compared with flight test data.

This validation process worked well for the NDARC development test cases: the UH-60A, CH-47D, XH-59A, and XV-15 rotorcraft. The results verified the utility of the models for rotor performance, engine performance, airframe aerodynamics, and component weights. Areas needing improvement and extension were identifed.

REFERENCES

1) Johnson, W.; Yamauchi, G.K.; and Watts, M.E. "NASA Heavy Lift Rotorcraft Systems Investigation." NASA TP 2005-213467, December 2005.

2) Yeo, H., and Johnson, W. "Aeromechanics Analysis of a Heavy Lift Slowed-Rotor Compound Helicopter." Journal of Aircraft, Vol. 44, No. 2 (March-April 2007).

3) Yeo, H.; Sinsay, J.D.; and Acree, C.W., Jr. "Blade Loading Criteria for Heavy Lift Tiltrotor Design." American Helicopter Society Southwest Region Technical Specialists' Meeting on Next Generation Vertical Lift Technologies, Dallas, TX, October 2008.

4) Johnson, W. "Influence of Lift Offset on Rotorcraft Performance." NASA TP 2009-215404, November 2009.

5) Acree, C.W., Jr.; Yeo, H.; and Sinsay, J.D. "Performance Optimization of the NASA Large Civil Tiltrotor." Royal Aeronautical Society International Powered Lift Conference, London, UK, July 2008.

6) Johnson, W. "NDARC — NASA Design and Analysis of Rotorcraft. Theoretical Basis and Architecture." American Helicopter Society Aeromechanics Specialists' Conference, San Francisco, CA, January 20-22, 2010.

7) Johnson, W. "NDARC, NASA Design and Analysis of Rotorcraft." NASA TP 2009-215402, December 2009.

8) Davis, S.J. "Predesign Study For a Modern 4-Bladed Rotor For the RSRA." NASA CR 166155, March 1981.

9) Howlett, J.J. "UH-60A Black Hawk Engineering Simulation Program: Volume II — Background Report." NASA CR 166309, CR 166310, December 1981.

10) Tarzanin, F.J., and Ranieri, J. "Investigation of the Effect of Torsional Natural Frequency on Stall-Induced Dynamic Loading." USAAMRDL TR 73-94, February 1974.

11) Bender, G.L.; Yamakawa, G.M.; Herbst, M.K.; Sullivan, P.J.; Robbins, R.D.; and Williams, R.A. "Airworthiness and Flight Characteristics Test (A&FC) of the CH-47D Helicopter." USAAEFA Project No. 82-07, February 1984.

12) Pleasants, W.A., III. "A Rotor Technology Assessment of the Advancing Blade Concept." NASA TM 84298, January 1983.

13) Ruddell, A.J. "Advancing Blade Concept (ABC) Technology Demonstrator." USAAVRADCOM TR 81-D-5, April 1981.

14) Acree, C.W., Jr. "An Improved CAMRAD Model for Aeroelastic Stability Analysis of the XV-15 With Advanced Technology Blades." NASA TM 4448, March 1993.

15) Bell Helicopter Company. "V/STOL Tilt-Rotor Study, Task II. Research Aircraft Design." NASA CR 114442, June 1972.

16) Maisel, M.D. "Tilt Rotor Research Aircraft Familiarization Document." NASA TM X-62407, January 1975.

17) Johnson, W. "Technology Drivers in the Development of CAMRAD II." American Helicopter Society Aeromechanics Specialists Conference, San Francisco, CA, January 1994.

18) Johnson, W. "Rotorcraft Aeromechanics Applications of a Comprehensive Analysis." HeliJapan 1998: AHS International Meeting on Rotorcraft Technology and Disaster Relief, Gifu, Japan, April 1998.

19) Bousman, W.G., and Kufeld, R.M. "UH-60A Airloads Catalog." NASA TM 2005-212827, August 2005.

20) Yeo, H.; Bousman, W.G.; and Johnson, W. "Performance Analysis of a Utility Helicopter With Standard and Advanced Rotors." Journal of the American Helicopter Society, Vol. 49, No. 3 (July 2004).

21) Gerdes, W.H.; Jackson, M.E.; and Beno, E.A. "Directional Control Developmental Experiences Associated With the UH-60A Utility Helicopter." USAAVRADCOM TR 82-D-26, May 1983.

22) Marshall, A.R., Jr.; MacMullin, R.; Lockwood, R.A.; Reynolds, T.L.; Tavares, E.J.; Buckanin, R.M.; Skinner, G.L.; Herbst, M.K.; Cassil, C.E.; Sullivan, P.J.; and Williams, R.A. "Airworthiness and Flight characteristics Test of a Sixth Year Production UH-60A." USAAFEA Project No. 83-24, June 1985.

23) Nagata, J.I.; Piotrowski, J.L.; Young, C.J.; Lewis, W.D.; Losier, P.W.; and Lyle, J.A. "Baseline Performance Verification of the 12th Year Production UH-60A Black Hawk Helicopter." USAAEFA Project No. 87-32, January 1989.

24) "System Specification for Utility Tactical Transport Aircraft System (UTTAS)." AMC-SS-2222-10000D, November 1975.

25) Arents, D.N. "An Assessment of the Hover Performance of the XH-59A Advancing Blade Concept Demonstration Helicopter." USAAMRDL TN-25, May 1977.

26) Felker, F.F.; Betzina, M.D.; and Signor, D.B. "Performance and Loads Data from a Hover Test of a Full-Scale XV-15 Rotor." NASA TM 86833, November 1985.

27) Arrington, L.; Kumpel, M.; Marr, R.; and McEntire, K. "XV-15 Tiltrotor Research Aircraft Flight Test Data Report." NASA CR 177406, June 1985.

28) Acree, C.W., Jr. "JVX Proprotor Performance Calculations and Comparisons with Hover and Airplane-Mode Test Data." NASA/TM–2009-215380, April 2009.

NOMENCLATURE

A	disk area
$c_{d\,\mathrm{mean}}$	profile power mean drag coefficient, $C_{Po} = (\sigma/8)c_{d\,\mathrm{mean}}F_P$
C_T/σ	thrust coefficient divided by solidity, $T/\rho A(\Omega R)^2\sigma$
$(C_T/\sigma)_s$	stall inception blade loading
C_P	power coefficient, $P/\rho A(\Omega R)^3$
C_W/σ	design blade loading, $W/\rho A V_{\mathrm{tip}}^2\sigma$
D	drag
D/q	drag area
DL	download
F_P	profile power factor, function of μ and μ_z
K_{int}	rotor wake-induced interference velocity factor
L	rotor wind axis lift force
L/D_e	rotor effective lift-to-drag ratio, $LV/(P+XV)$
L/D	aircraft lift-to-drag ratio, WV/P
M_{at}	advancing tip Mach number
M_{dd}	drag divergence Mach number
M_{tip}	rotor tip Mach number
P	power
P_i	rotor induced power
P_o	rotor profile power
P_p	rotor parasite power, $-XV$
q	dynamic pressure, $\frac{1}{2}\rho V^2$
R	blade radius
sfc	specific fuel consumption, $\dot{w}/P$ (conventional units)
T	rotor thrust
T_{design}	tail rotor design thrust
$\dot{w}$	fuel flow (conventional units)
W	weight
V	flight speed
V_{tip}	rotor tip speed, ΩR
X	rotor wind axis drag force
κ	induced power factor, $P_i = \kappa P_{\mathrm{ideal}}$
μ	advance ratio (edgewise)
μ_z	axial advance ratio
ρ	density
σ	solidity (ratio blade area to disk area)
Ω	rotor rotational speed
DGW	design gross weight
GW	gross weight
IGE	in ground effect
IRP	intermediate rated power
ISA	International Standard Atmosphere
ISO	International Organization for Standardization
MCP	maximum continuous power
MRP	maximum rated power
OEI	one engine inoperative
OGE	out of ground effect
ROC	rate of climb
SDGW	structural design gross weight
SLS	sea level standard

Table 1. Principal aircraft parameters.

	UH60A		CH47D	XH59A	XV15
Configuration	Helicopter		Tandem	Coaxial	Tiltrotor
disk loading (lb/ft^2)	7.29		6.62	8.84	13.24
power loading (hp/ft^2)	5.14		3.92	5.21	4.19
Rotor	main	tail			
C_W/σ at design gross weight	0.087	0.103	0.072	0.069	0.114
radius (ft)	26.833	5.5	30	18	12.5
solidity σ (thrust-weighted)	0.0832	0.1875	0.0849	0.0636	0.0890
number of blades	4	4	3	3	3
tip speed (ft/sec)	725	686	707	650	740
cruise tip speed (ft/sec)	725	686	707	650	600
flap frequency (/rev)	1.035	1.140	1.020	1.450	1.020
Lock number	7.07	2.01	8.95	4.20	3.71
Wing, area (ft^2)					168.88
span (ft)					32.17
aspect ratio					6.13
Horizontal tail, area (ft^2)	45.00			60.00	50.25
span (ft)	14.33			15.50	12.83
aspect ratio	4.56			4.00	3.28
tail length (ft)	28.36			20.30	21.96
Vertical tail, area (ft^2)	32.30			30.00	50.50
span (ft)	8.17			12.00	15.36
aspect ratio	2.07			4.80	4.67
tail length (ft)	27.69			20.30	22.80
Engines	T700-GE-700		T55-L-712	PT6T-3	LTC1K-4K
number of engines	2		2	1	2
takeoff power (hp)	IRP = 1560		MRP = 4204	IRP = 1726	MRP = 1550
MCP power (hp)	1313		3006	1452	1250
MCP specific power (hp/lb/sec)	120		119	100	112
MCP SLS sfc (lb/hp-hr)	0.474		0.561	0.599	0.622
weight/power (lb/hp)	0.27		0.18	0.39	0.32
drive system limit (hp)	2828		7533	1500	2332
Design gross weight	16500		33000	9000	13000
structural design gross weight	16825		33000	9000	13000
maximum takeoff weight	22000		50000	9000	15000
weight empty	11205		23263	8051	10101
Cruise drag D/q (ft^2)	25.69		50.93	14.78	9.25
fuselage	5.28		11.37	2.01	1.56
fuselage fittings & fixtures	5.31		3.00		3.00
rotor 1 hub	5.83		7.70	3.72	
rotor 1 pylon	4.14		2.50		0.76
rotor 2 hub	2.90		7.70	3.72	0.00
rotor 2 pylon			10.13		0.76
horizontal tail	0.60			0.47	0.63
vertical tail	0.60			0.48	0.36
engine nacelle	1.03		2.90	0.89	
other			landing gear 5.63	contingency 3.50	wing 2.18
$C_D = (D/q)/A_{\text{ref}}$	0.011		0.010	0.015	0.009
$(D/q)/(W/1000)^{2/3}$	3.27		3.75	3.42	1.52
Download DL/T	0.036		0.056	0.025	0.108
Fuselage, length (ft)	41.33		50.75	40.50	41.00
width (ft)	7.75		9.00	6.08	5.50
height (ft)	5.75		8.17	6.08	6.17
Fuel tank capacity (lb)	2338		6695	1666	1401
Rotor separation	mr/tr=0.233 ft		$x/D = 0.352$	$z/D = 0.069$	$y/D = 1.287$
Landing gear	fixed		fixed	retractable	retractable

Table 2. Component weight calibration factors.

	UH-60A	CH-47D	XH-59A	XV-15
structure				
wing group				
basic structure				0.98 *
rotor group				
blade assembly	1.02	0.94	1.00 **	0.93
hub & hinge	0.98	1.03	1.00 **	0.88
fairing/spinner				0.97
empennage group				
horizontal tail	0.94		1.03	1.42
vertical tail	2.47		1.65	0.60
tail rotor	1.18			
fuselage group				
basic	1.03	1.03	1.06	1.03
alighting gear group				
basic	0.74	1.00	0.98	0.96
engine section or nacelle group				
engine support + air induction group	1.27	0.89	1.71	0.85
engine cowling	0.91	0.93	0.99	0.56
propulsion group				
engine system				
accessories	0.71	0.74	1.44	0.62
fuel system				
tanks and support	0.83	1.04	0.97	2.25
drive system				
gear boxes + rotor shaft	0.91	0.90	1.06	1.35
transmission drive	0.85	0.79		0.62
systems and equipment				
fixed wing flight controls	1.15		0.57	0.72
rotary wing flight controls				
non-boosted	1.17	0.99	1.08	0.94
boost mechanisms + hydraulic	1.17	1.59	1.13	1.08
boosted	1.06	0.77	2.29	1.02

* model calibrated for XV-15 wing

** model calibrated for XH-59A rotor

Table 3a. Rotor performance model parameters: induced power $P_i = \kappa P_{\text{ideal}}$

		UH-60A	CH-47D	XH-59A	XV-15
Induced velocity factors					
hover	κ_{hover}	1.125	1.15	1.15	1.05
axial climb	κ_{climb}	1.125	1.12	1.12	1.05
axial cruise (propeller)	κ_{prop}	2.00	1.12	10.00	7.00
edgewise flight (helicopter)	κ_{edge}	2.00	2.00	10.00	2.00
Variation with thrust					
$\Delta_h = C_T/\sigma - (C_T/\sigma)_{H\,\text{ind}}$	$(C_T/\sigma)_{H\,\text{ind}}$	0.05	0.06	0.08	0.11
$\kappa_h = \kappa_{\text{hover}} + k_{h1}\Delta_h + k_{h2}\Delta_h^2$	k_{h1}	0	1.5	1.8	-0.5
coefficient	k_{h2}	80	0	-8	30
$\Delta_p = C_T/\sigma - (C_T/\sigma)_{P\,\text{ind}}$	$(C_T/\sigma)_{P\,\text{ind}}$	0.08	0.06	0.08	0.11
$\kappa_p = \kappa_{\text{prop}} + k_{p1}\Delta_p + k_{p2}\Delta_p^2$	k_{p1}	0	1.5	1.8	100
coefficient	k_{p2}	0	0	-8	2000
Variation with lift offset, $f_{\text{off}} = 1 - k_{o1}(1 - e^{-k_{o2}o_x})$					
coefficient	k_{o1}			0.6	
exponent factor	k_{o2}			8	
Constant in transition from hover to climb	M_{axial}	1.176	1.176	1.176	1.176
Exponent in transition from hover to climb	X_{axial}	0.65	0.65	0.65	0.65
Variation with axial velocity					
axial advance ratio for κ_{prop}	$\mu_{z\,\text{prop}}$	1.00	1.00	0.15	0.50
$\kappa_{\text{axial}} = \kappa_h + k_{a1}\mu_z + S_a(k_{a2}\mu_z^2 + k_{a3}\mu_z^{X_a})$	k_{a1}	0	0	8	0
coefficient	k_{a2}	0	0	0	0
coefficient	k_{a3}	0	0	0	1
exponent	X_a	4.5	4.5	4.5	1.4
Variation with edgewise velocity					
advance ratio for κ_{edge}	μ_{edge}	0.35	0.35	0.60	0.50
$\kappa = \kappa_{\text{axial}} + k_{e1}\mu + S_e(k_{e2}\mu^2 + k_{e3}\mu^{X_e})$	k_{e1}	0.8	0	1.5	0
coefficient	k_{e2}	0	0	0	0
coefficient	k_{e3}	1	1	1	1
exponent	X_e	4.5	4	4.5	3
Minimum κ	κ_{min}	1.65	1.05	1.00	1.00
Maximum κ	κ_{max}	10	10	40	40
Twin rotors					
model		none	tandem	coaxial	tiltrotor
ideal induced velocity correction for hover	$\kappa_{h\,\text{twin}}$		1.00	1.00	1.00
ideal induced velocity correction for forward flight	$\kappa_{f\,\text{twin}}$		0.85	0.86	1.00
constant in hover to forward flight transition	C_{twin}		1	1	1
coaxial rotor nonuniform disk loading factor	$\overline{\alpha}$				1.05

Table 3b. Rotor performance model parameters: profile power $C_{Po} = (\sigma/8)c_{d\,\text{mean}}F_P$, $c_{d\,\text{mean}} = c_{d\,\text{basic}} + c_{d\,\text{stall}} + c_{d\,\text{comp}}$.

		UH-60A	CH-47D	XH-59A	XV-15
Basic model					
$c_{d\,\text{basic}} = c_{dh} + (c_{dp} - c_{dh})\frac{2}{\pi}\tan^{-1}(\lvert\mu_z\rvert/\lambda_h)$					
minimum profile drag $\Delta = \lvert C_T/\sigma - (C_T/\sigma)_{D\min}\rvert$	$(C_T/\sigma)_{D\min}$	0.04	0.07	0.00	0.02
$c_{dh} = d_{0\,\text{hel}} + d_{1\,\text{hel}}\Delta + d_{2\,\text{hel}}\Delta^2 + d_{\text{sep}}\Delta_{\text{sep}}^{X_{\text{sep}}}$	$d_{0\,\text{hel}}$	0.0090	0.0085	0.0105	0.0092
coefficient	$d_{1\,\text{hel}}$	0	0	0	0
coefficient	$d_{2\,\text{hel}}$	0.9	0	0	0.55
$c_{dp} = d_{0\,\text{prop}} + d_{1\,\text{prop}}\Delta + d_{2\,\text{prop}}\Delta^2 + d_{\text{sep}}\Delta_{\text{sep}}^{X_{\text{sep}}}$	$d_{0\,\text{prop}}$	0.0090	0.0085	0.0105	0.0088
coefficient	$d_{1\,\text{prop}}$	0	0	0	0
coefficient	$d_{2\,\text{prop}}$	0.9	0	0	0
separation, $\Delta_{\text{sep}} = \lvert C_T/\sigma\rvert - (C_T/\sigma)_{\text{sep}}$	$(C_T/\sigma)_{\text{sep}}$	0.06	0.07	0.07	0.07
factor	d_{sep}	20	7	8	5
exponent	X_{sep}	3	3	3	3
Stall model, $c_{d\,\text{stall}} = d_{s1}\Delta_s^{X_{s1}} + d_{s2}\Delta_s^{X_{s2}}$					
$\Delta_s = \lvert C_T/\sigma\rvert - (f_s/f_{\text{off}})(C_T/\sigma)_s$	$(C_T/\sigma)_s$	figure 9	figure 25	figure 37	figure 53
factor	f_s	1	1	1	1
coefficient	d_{s1}	5	4	12	2
coefficient	d_{s2}	40	120	40	600
exponent	X_{s1}	2	2	2	2
exponent	X_{s2}	3	3	3	4
variation with lift offset, $f_{\text{off}} = 1 - d_{o1}(1 - e^{-d_{o2}o_x})$					
coefficient	d_{o1}			0.6	
factor	d_{o2}			7	
Compressibility model, $c_{d\,\text{comp}} = d_{m1}\Delta M + d_{m2}\Delta M^{X_m}$					
$\Delta M = M_{at} - M_{dd}$, $M_{dd} = M_{dd\,0} - M_{dd\,c_\ell}c_\ell$					
coefficient	d_{m1}	0.005	0.005	0.015	0.005
coefficient	d_{m2}	0.9	1.0	1.0	2.0
exponent	X_m	3	3	3	3
drag divergence Mach number at zero lift	$M_{dd\,0}$	0.68	0.71	0.75	0.70
derivative	$M_{dd\,c_\ell}$	0	0	0	0

Table 4. Helicopter design criteria.

	Segment	kind	length min/nm	speed knots	altitude ft	temp deg F	weight lb	power
primary mission: takeoff at DGW, 2.3 hr endurance, 4k/95								
1	warm-up	idle	8	0	4000	95	2640 payload, mission fuel	idle
2	max power	time	20	—	4000	95		100% MCP
3	cruise	time	80	145	4000	95		MCP
4	reserve	time	30	145	4000	95		MCP
fuel tank design: takeoff at DGW, 3.0 hr endurance, 4k/95								
1	warm-up	idle	8	0	4000	95	max fuel, payload fallout	idle
2	max power	time	20	—	4000	95		100% MCP
3	cruise	time	122	145	4000	95		MCP
4	reserve	time	30	145	4000	95		MCP
alternate endurance: takeoff at SDGW, 2.3 hr endurance, SLS								
1	warm-up	idle	8	0	0	59	2640 payload, mission fuel	idle
2	max power	time	20	—	0	59		100% MCP
3	cruise	time	80	145	0	59		MCP
4	reserve	time	30	145	0	59		MCP
point design conditions								
	hover vertical rate-of-climb			≥ 455-500 ft/min	4000	95	DGW	95% IRP
	maximum speed			≥ 145-175	4000	95	DGW	100% MCP
	maximum alternate gross weight			0	4000	95	max GW	100% IRP
	OEI level flight speed			≥ 100	4000	95	DGW	100% IRP OEI
	OEI service ceiling (ROC=100 ft/min)			min power	≥ 5000	95	DGW	100% IRP OEI
	OEI hover IGE			0	IGE 4000	95	DGW less payload	100% IRP OEI

Table 5. Helicopter design demonstration.

Size	baseline	rotor	rotor	engine	engine
Technology factors	calibrated	calibrated	1.0	calibrated	1.0
Engine		fixed	fixed	sized	sized
Main rotor		size R	size R	fix DL	fix DL
Configuration	Helicopter	Helicopter	Helicopter	Helicopter	Helicopter
Disk loading (lb/ft^2)	7.3	7.1	6.8	7.3	7.3
Power loading (lb/ft^2)	5.1	5.2	5.3	5.1	5.1
Weight					
design gross weight	16500	16772	17132	17256	17899
structural design gross weight	16825	17425	17778	17930	18597
maximum takeoff weight	22000	21146	21584	21918	22751
weight empty	11205	11192	11574	11603	12168
WE/DGW (%)	67.9	66.7	67.6	67.2	68.0
Fuel tank capacity (lb)	2338	2808	2780	2902	3004
Engines					
number of engines	2	2	2	2	2
takeoff power, IRP (hp)	1560	1560	1560	1684	1746
MCP power (hp)	1313	1313	1313	1378	1428
MCP specific power (hp/lb/sec)	120	120	120	121	122
MCP SLS sfc (lb/hp-hr)	0.474	0.474	0.474	0.473	0.472
engine weight (lb)	437	437	437	458	475
weight/power (lb/hp)	0.27	0.27	0.27	0.27	0.27
drive system limit (hp)	2828	2963	2963	3368	3492
Main rotor					
Disk loading (lb/ft^2)	7.3	7.1	6.8	7.3	7.3
C_W/σ at DGW	0.087	0.087	0.087	0.087	0.087
radius (ft)	26.83	27.39	28.33	27.43	27.94
solidity σ (thrust-weighted)	0.0832	0.0811	0.0774	0.0832	0.0832
Tail rotor					
Disk loading (lb/ft^2)	17.4	17.4	17.4	17.4	17.4
C_W/σ at T_{design}	0.103	0.103	0.103	0.103	0.103
T_{design}	1650	1645	1652	1722	1787
radius (ft)	5.50	5.49	5.50	5.62	5.72
solidity σ (thrust-weighted)	0.1875	0.1875	0.1875	0.1875	0.1875
Cruise drag D/q (ft^2)	25.69	26.32	27.57	26.84	287.90
fuselage	5.28	5.36	5.55	5.39	5.48
fuselage fittings & fixtures	5.31	5.41	5.58	5.42	5.51
rotor 1 hub	5.83	6.07	6.50	6.09	6.32
rotor 1 pylon	4.14	4.28	4.64	4.60	5.04
rotor 2 hub	2.90	2.89	2.90	3.03	3.14
horizontal tail	0.60	0.63	0.67	0.63	0.65
vertical tail	0.60	0.63	0.67	0.63	0.65
engine nacelle	1.03	1.03	1.05	1.06	1.11
$C_D = (D/q)/A_{ref}$	0.0114	0.0112	0.0109	0.0114	0.0114
$(D/q)/(W/1000)^{2/3}$	3.27	3.44	3.45	3.43	3.48
Download DL/T	0.036	0.034	0.033	0.034	0.034
Fuselage					
length (ft)	41.33	42.06	43.33	42.24	43.02
width (ft)	7.75	7.75	7.75	7.75	7.75
height (ft)	5.75	5.75	5.75	5.75	5.75
Cost, aircraft \$M	12.8	12.8	12.9	13.1	13.5
maintenance \$/hr	692	692	701	717	742

Table 6. Endurance mission.

	Segment	kind	length min/nm	speed knots	altitude ft	temp deg F	weight lb	power
endurance mission: takeoff at DGW, 4k/95								
1	warm-up	idle	5	0	4000	95	fallout fuel or payload	idle
2	max power	time	5	—	4000	95		100% MRP
3	cruise	time	max	V_{be}	4000	95		MCP
4	reserve	time	30	V_{be}	4000	95		MCP

Table 7. Tiltrotor design criteria.

	Segment	kind	length min/nm	speed knots	altitude ft	temp deg F	weight lb	power
primary mission: takeoff at DGW (fallout), 300 nm range, 10k/ISA cruise, 10% fuel reserve								
1	warm-up	idle	5	0	0	59	1200 payload, mission fuel	idle
2	hover	time	5	—	0	59		MRP
3	climb	dist	—	best climb	climb	ISA		MCP
4	cruise	dist	300	V_{br}	10000	ISA		MCP
fuel tank design: takeoff at DGW, 2.5 hr endurance, 10k/ISA cruise, 10% fuel reserve								
1	warm-up	idle	5	0	0	59	max fuel, payload fallout	idle
2	hover	time	5	—	0	59		MRP
3	climb	time	20	best climb	climb	ISA		MCP
4	cruise	time	120	V_{be}	10000	ISA		MCP
point design conditions								
	maximum takeoff weight			0	0	59	max GW	100% MRP
	hover ceiling			0	≥8000	ISA	DGW	100% MRP
	maximum speed			≥ 225	0	59	DGW	100% MCP
	maximum speed			≥ 260	12000	ISA	DGW	100% MCP
	OEI level flight speed			≥ 150	12000	ISA	DGW	100% MCP

Table 8. Tiltrotor design demonstration: cruise tip speed variation.

design cruise tip speed (ft/sec)	740	700	650	600	550	500	450	400
Weight (lb)								
design gross weight	15054	14902	14828	14821	15224	16739	19603	24909
structural design gross weight	15182	15027	14952	14945	15358	16906	19838	25282
maximum takeoff weight	17098	16924	16838	16831	17465	19878	24300	32271
weight empty	11536	11438	11390	11386	11730	13043	15545	20244
Fuel tank capacity (lb)	1982	1925	1898	1896	1964	2198	2628	3375
Engines								
takeoff power, MRP (hp)	1929	1908	1898	1897	1991	2356	3059	4407
MCP power (hp)	1555	1539	1530	1530	1605	1900	2467	3554
MCP specific power (hp/lb/sec)	124.9	124.2	123.9	123.9	126.9	138.0	157.2	188.6
MCP SLS sfc (lb/hp-hr)	0.604	0.605	0.606	0.606	0.601	0.586	0.559	0.516
engine weight (lb)	616	609	606	606	636	753	977	1408
weight/power (lb/hp)	0.32	0.32	0.32	0.32	0.32	0.32	0.32	0.32
drive system limit (hp)	2902	2871	2855	2854	2995	3545	4603	6632
Rotor								
disk loading (lb/ft^2)	13.24	13.24	13.24	13.24	13.24	13.24	13.24	13.24
C_W/σ at DGW	0.1144	0.1144	0.1144	0.1144	0.1144	0.1144	0.1144	0.1144
radius (ft)	13.45	13.38	13.35	13.35	13.53	14.19	15.35	17.30
solidity σ (thrust-weighted)	0.0890	0.0890	0.0890	0.0890	0.0890	0.0890	0.0890	0.0890
number of blades	3	3	3	3	3	3	3	3
hover tip speed (ft/sec)	740	740	740	740	740	740	740	740
cruise tip speed (ft/sec)	740	700	650	600	550	500	450	400
Wing								
wing loading (lb/ft^2)	76.98	76.98	76.98	76.98	76.98	76.98	76.98	76.98
area (ft^2)	195.6	193.6	192.6	192.5	197.8	217.4	254.7	323.6
span (ft)	34.07	33.93	33.87	33.86	34.22	35.54	37.87	41.77
aspect ratio	5.94	5.95	5.95	5.96	5.92	5.81	5.63	5.39
Fuselage length (ft)	44.12	43.90	43.79	43.78	44.37	46.53	50.35	56.76
Cruise drag D/q (ft^2)	10.32	10.24	10.21	10.20	10.42	11.22	12.70	15.33
$C_D = (D/q)/A_{\text{ref}}$	0.0091	0.0091	0.0091	0.0091	0.0091	0.0089	0.0086	0.0081
$(D/q)/(W/1000)^{2/3}$	1.55	1.55	1.55	1.55	1.55	1.53	1.51	1.51
Cost, aircraft $M	13.2	13.1	13.0	13.0	13.5	15.1	18.4	24.5
maintenance $/hr	762	756	753	752	778	875	1055	1380
Cruise performance								
gross weight	14629	14486	14413	14404	14789	16255	19030	24184
power (hp)	859	830	807	785	790	867	1025	1327
V best range (knots)	212.3	213.4	213.7	212.8	212.8	215.3	219.6	225.9
total drag D/q (ft^2)	16.13	15.89	15.81	15.88	16.27	17.51	19.73	23.65
total drag (lb)	1817	1810	1805	1799	1844	2029	2378	3020
airframe L/D	8.05	8.00	7.98	8.01	8.02	8.01	8.00	8.01
propulsive efficiency	0.764	0.792	0.813	0.827	0.840	0.852	0.863	0.872
sfc (lb/hp-hr)	0.611	0.615	0.623	0.637	0.653	0.668	0.679	0.676
range for 1%GW	32.96	33.74	34.10	34.06	33.79	33.46	33.30	33.81
aircraft $L/D = VW/P$	5.55	5.71	5.86	5.99	6.11	6.19	6.25	6.32

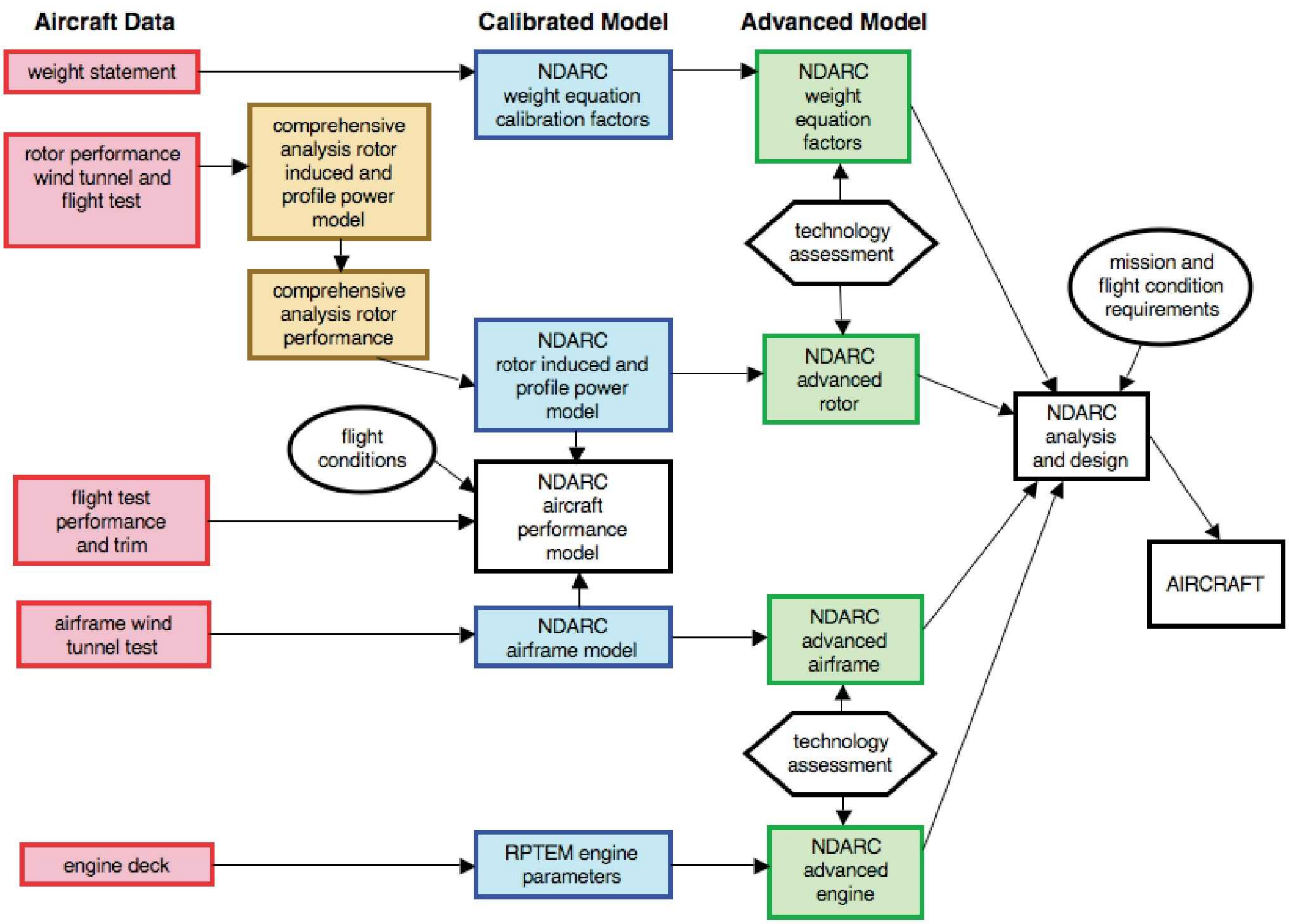

Figure 1. NDARC calibration and validation process.

UH-60A single-main rotor and tail-rotor helicopter

XH-59A coaxial lift-offset helicopter

CH-47D tandem helicopter

XV-15 tiltrotor aircraft

Figure 2. NDARC development test cases.

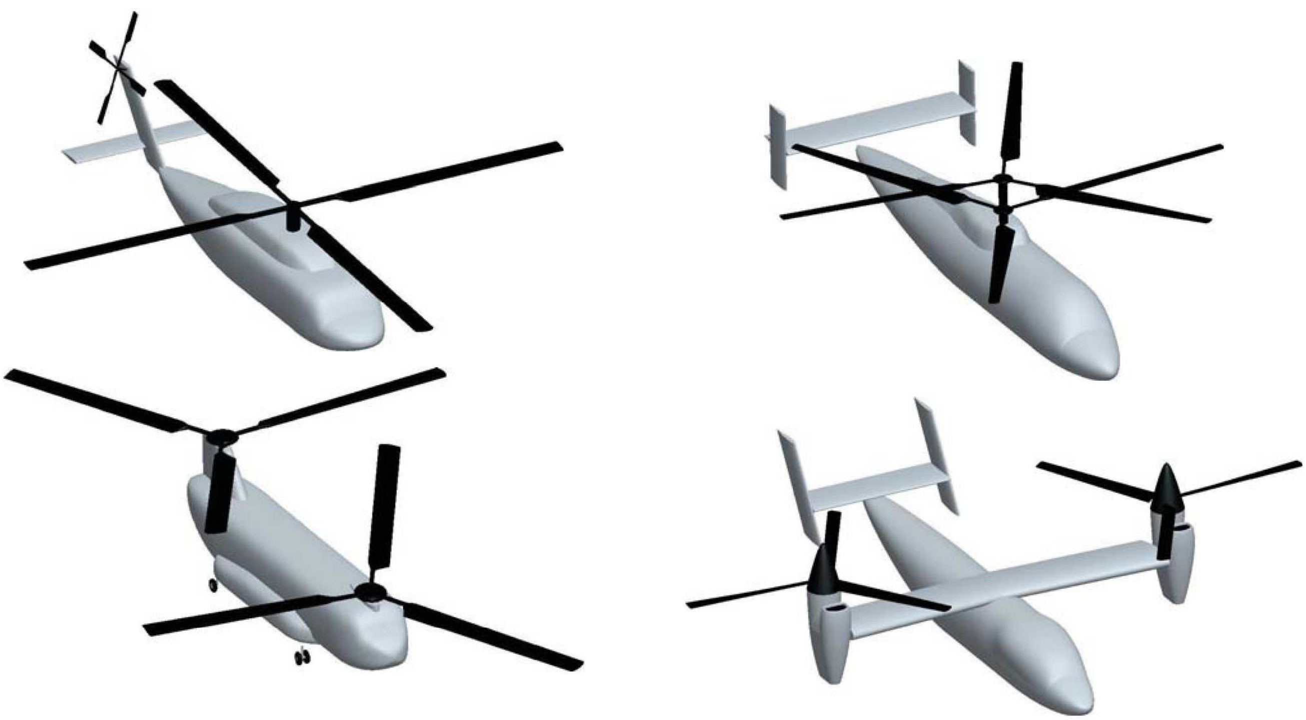

Figure 3. NDARC models for test cases.

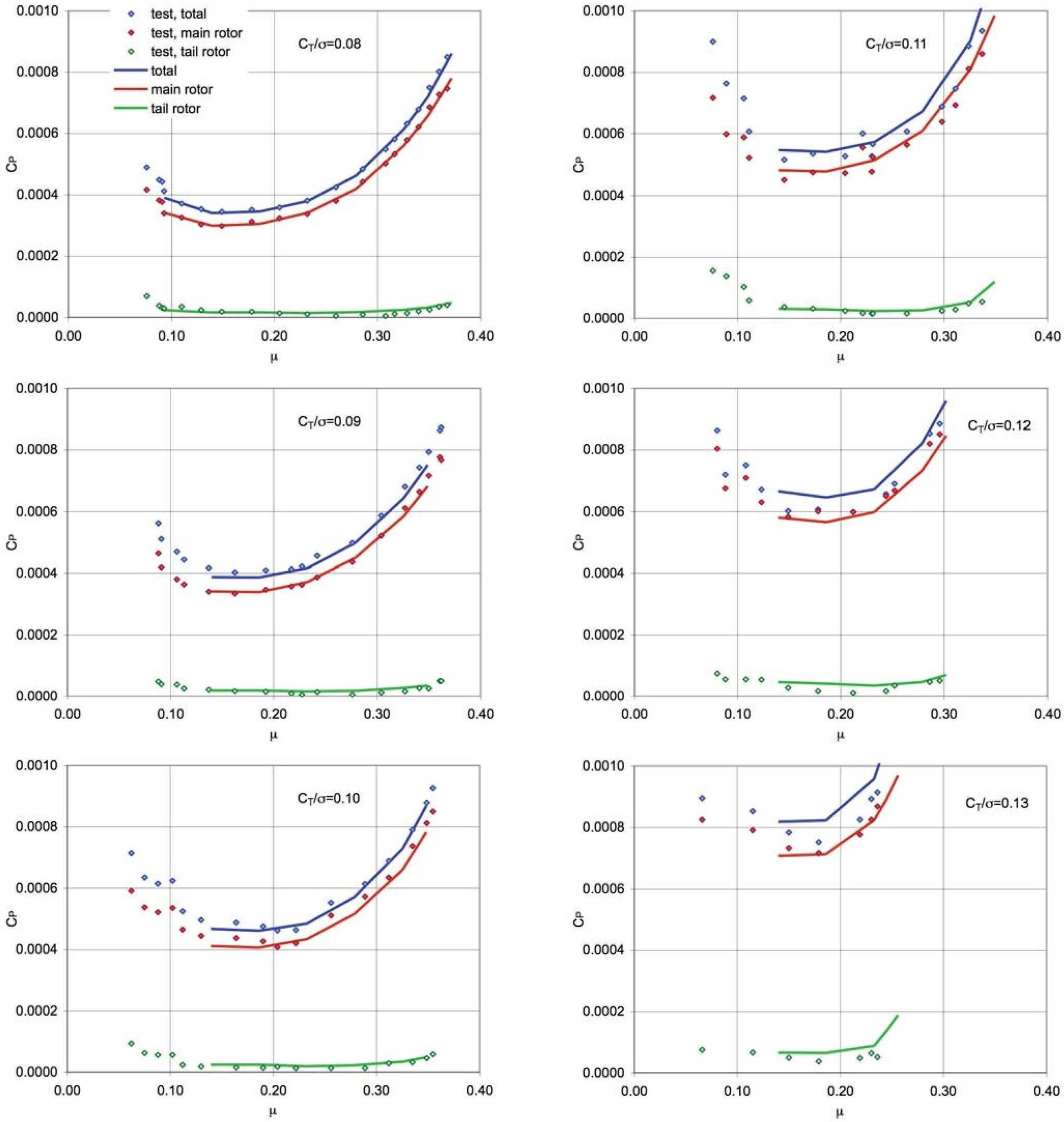

Figure 4. Comparison of UH-60A Airloads flight test performance with CAMRADII calculations.

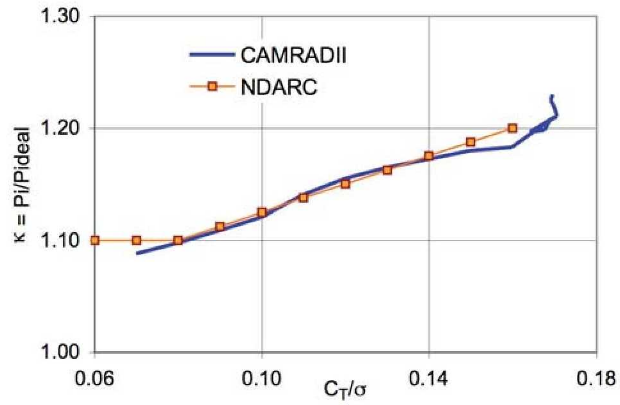

Figure 5. UH-60A rotor model: hover induced power.

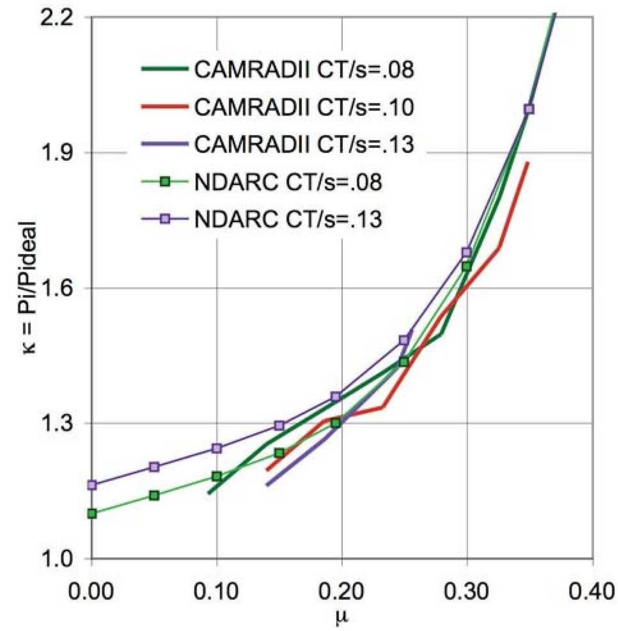

Figure 6. UH-60A rotor model: forward flight induced power.

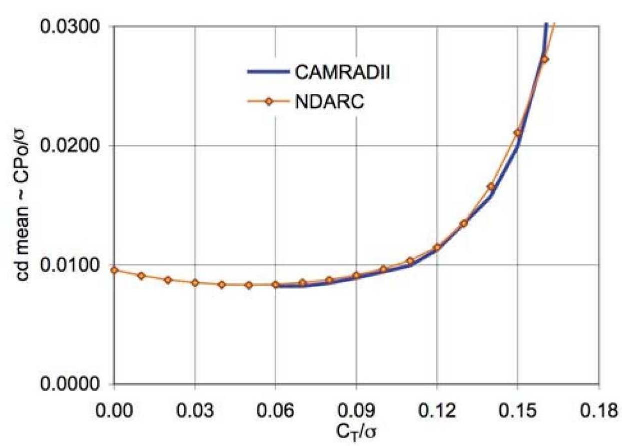

Figure 7. UH-60A rotor model: hover profile power.

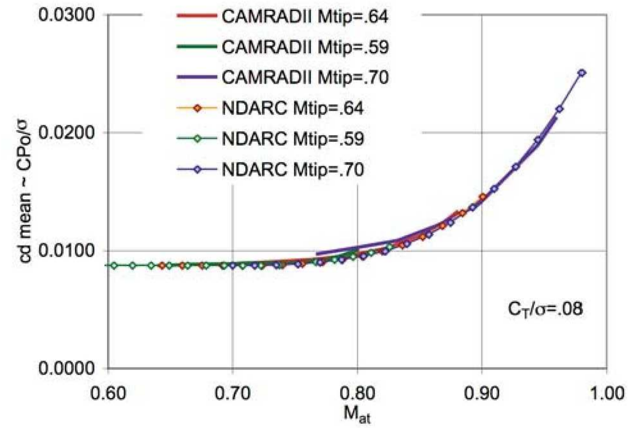

Figure 8. UH-60A rotor model: compressibility profile power.

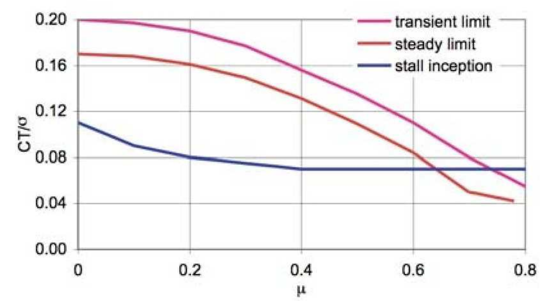

Figure 9. UH-60A rotor model: NDARC profile power stall loading $(C_T/\sigma)_s$.

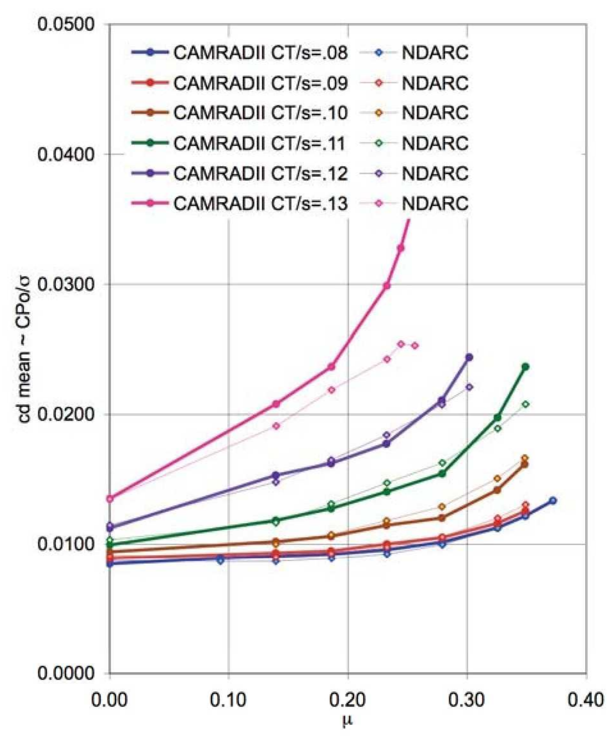

Figure 10. UH-60A rotor model: forward flight profile power.

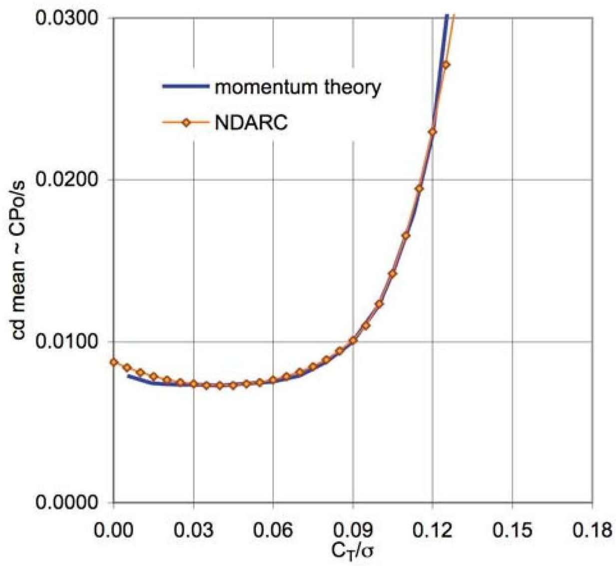

Figure 11. UH-60 tail rotor model: hover profile power.

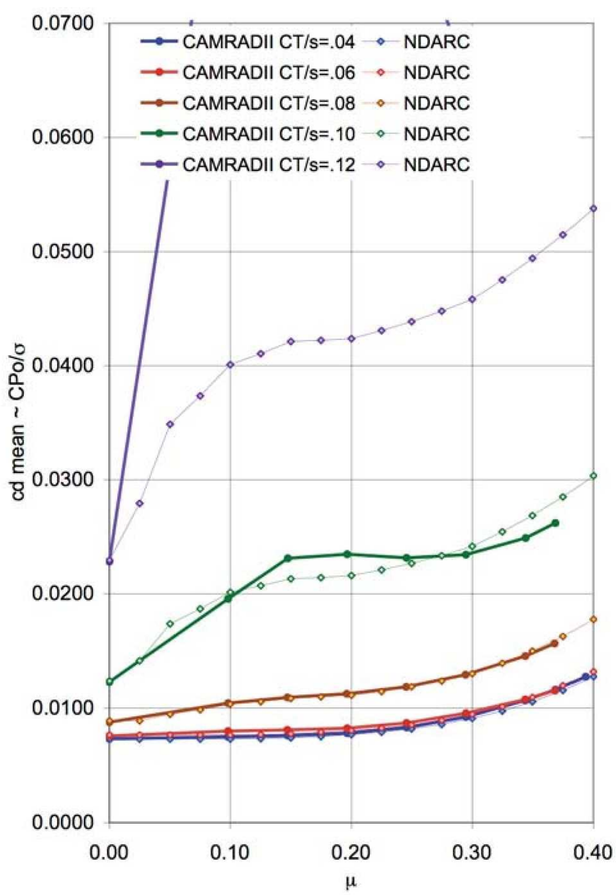

Figure 12. UH-60A tail rotor model: forward flight profile power.

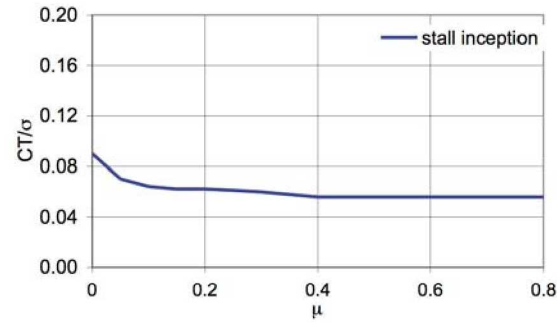

Figure 13. UH-60A tail rotor model: NDARC profile power stall loading $(C_T/\sigma)_s$.

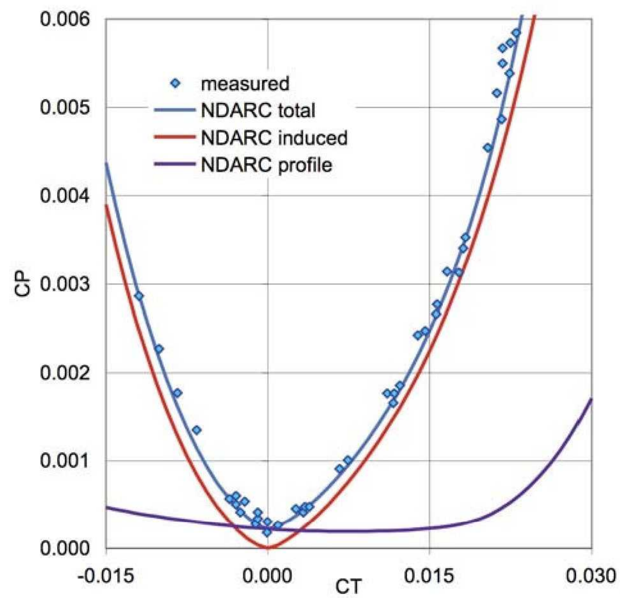

Figure 14. UH-60A tail rotor power in hover.

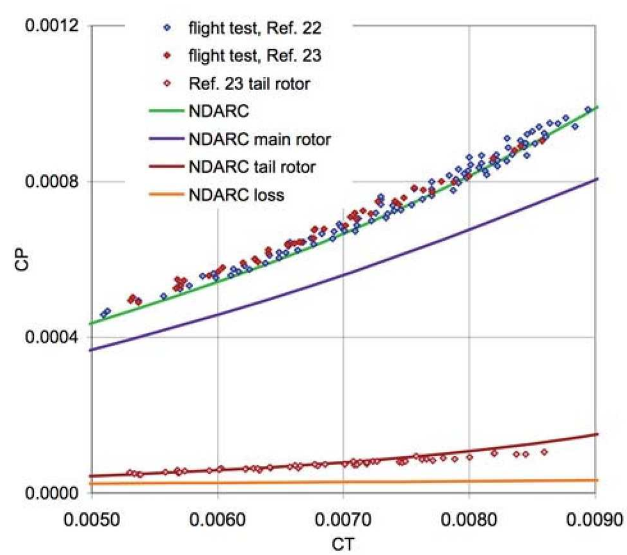

Figure 15. UH-60A hover performance, comparing NDARC calculations with flight test.

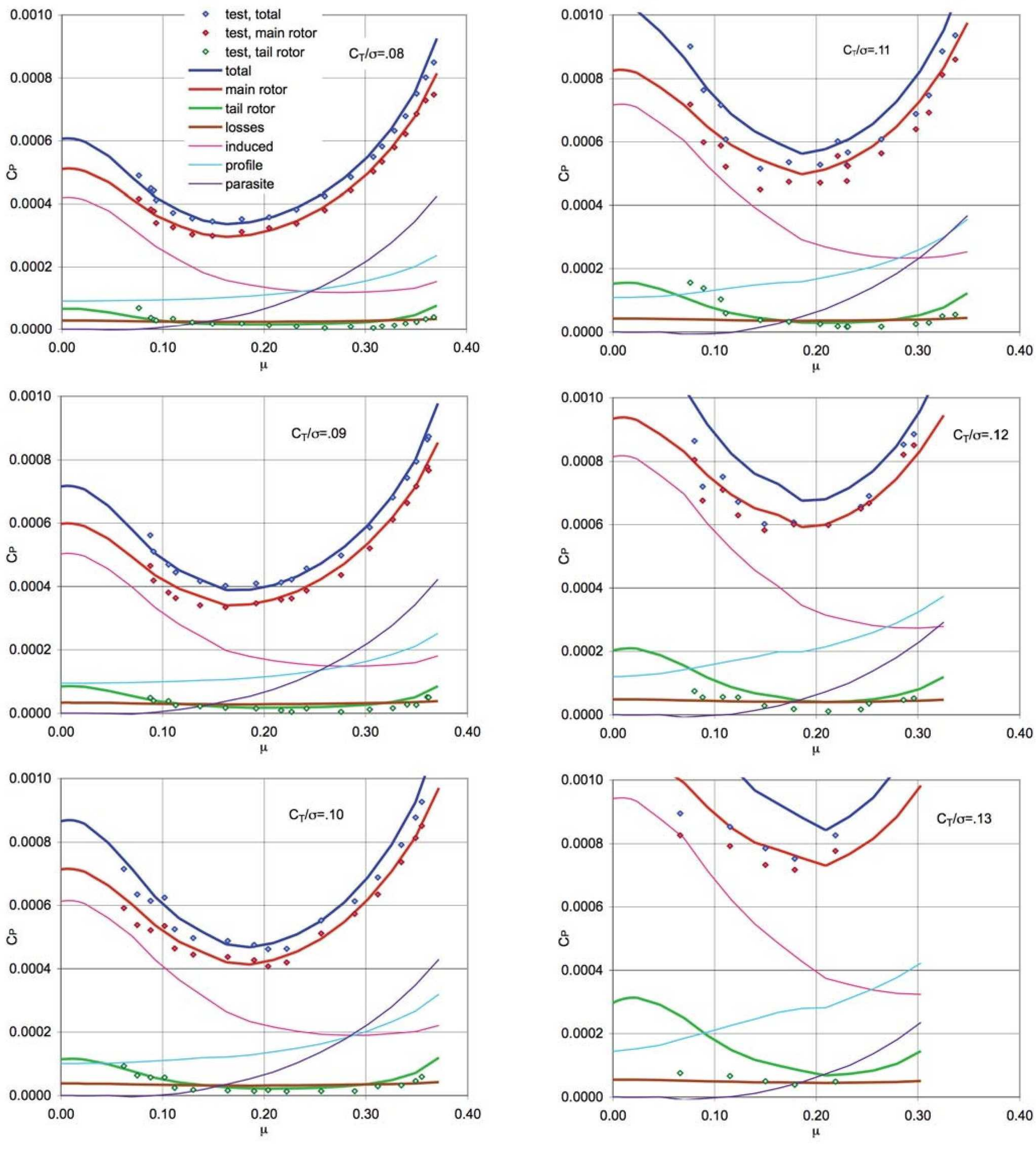

Figure 16. Comparison of UH-60A Airloads flight test performance with NDARC calculations.

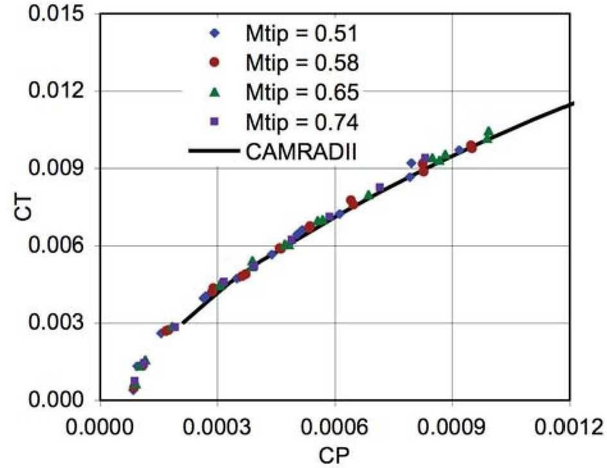

(a) single rotor on whirl stand

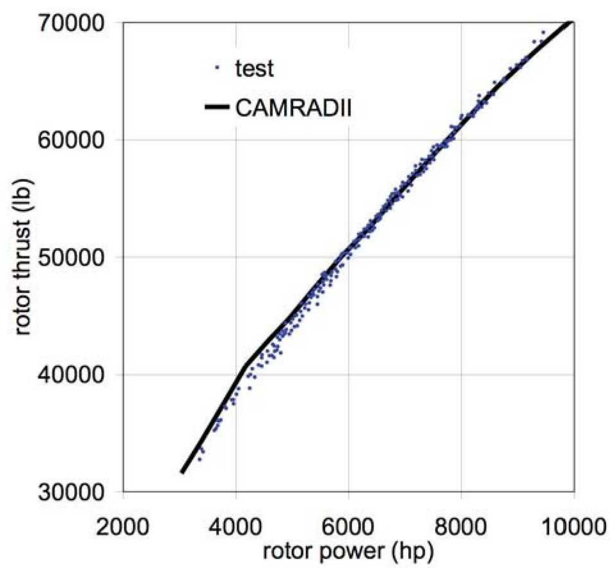

(b) tandem rotors in flight

Figure 17. Comparison of CH-47D hover performance with CAMRADII calculations.

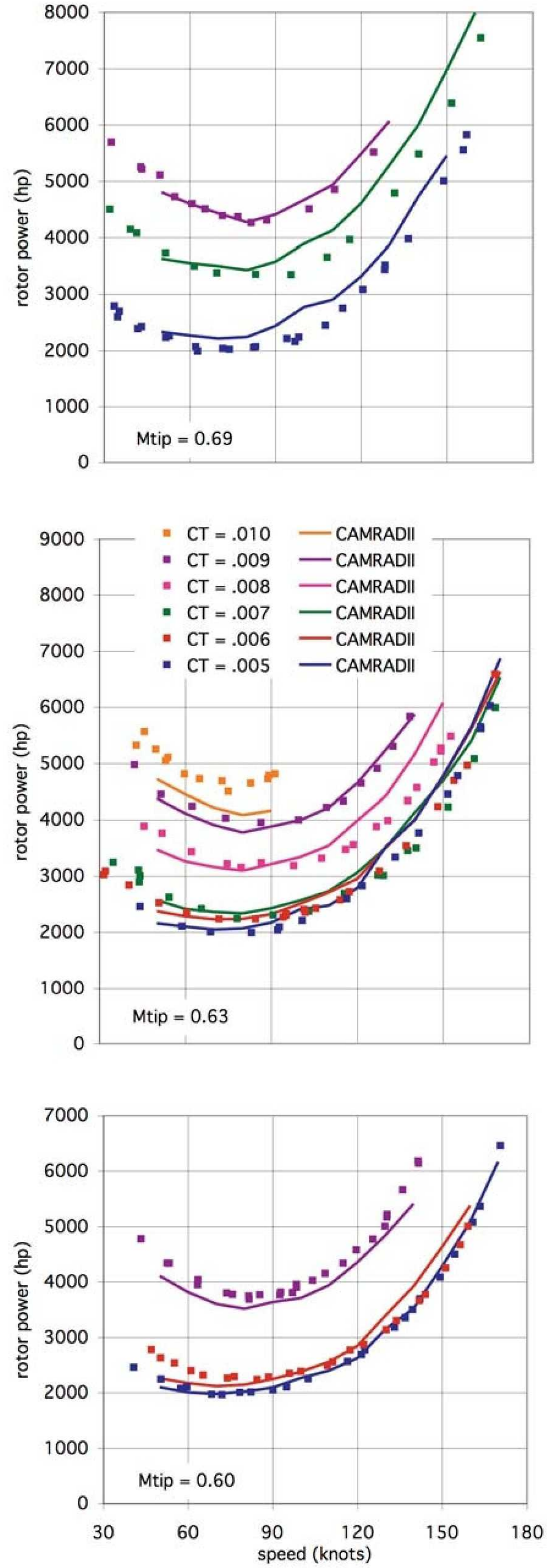

Figure 18. Comparison of CH-47D forward flight performance with CAMRADII calculations.

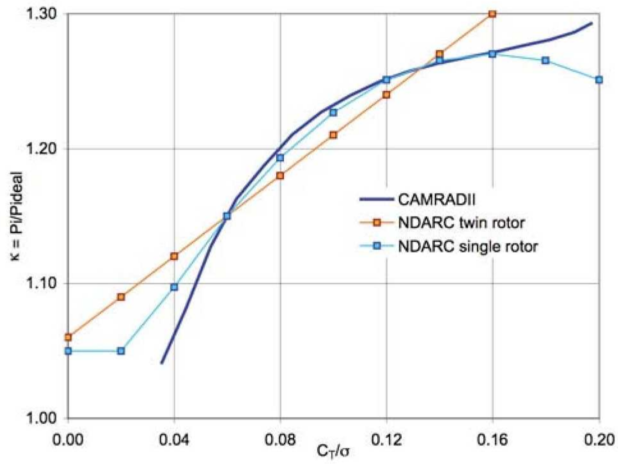

Figure 19. CH-47D rotor model: hover induced power for single rotor.

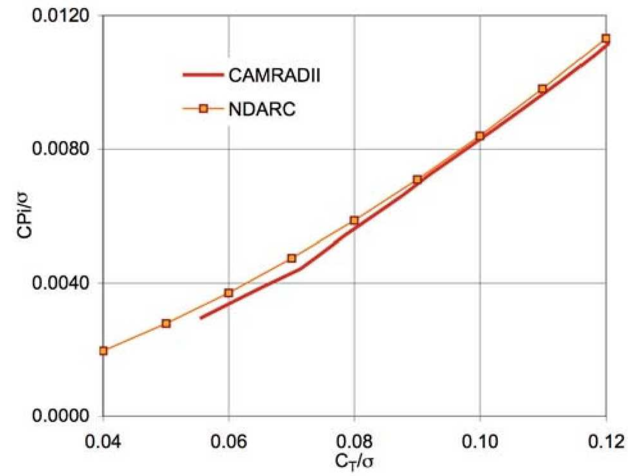

Figure 21. CH-47D rotor model: hover induced power for tandem rotors.

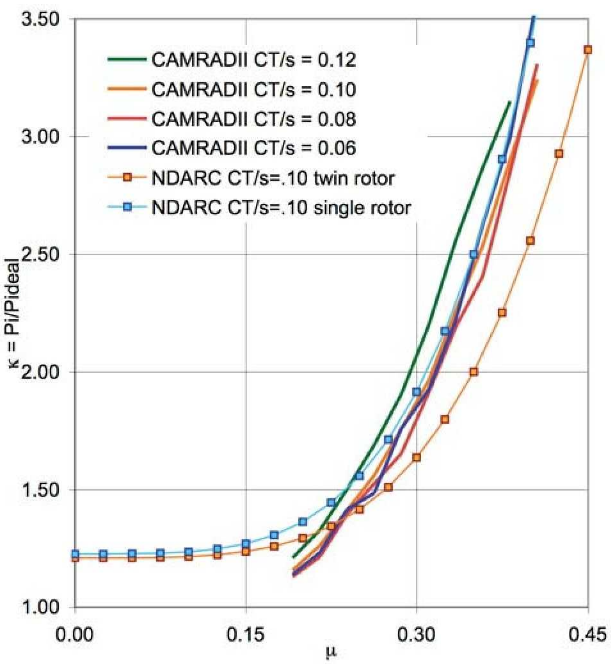

Figure 20. CH-47D rotor model: forward flight induced power for single rotor.

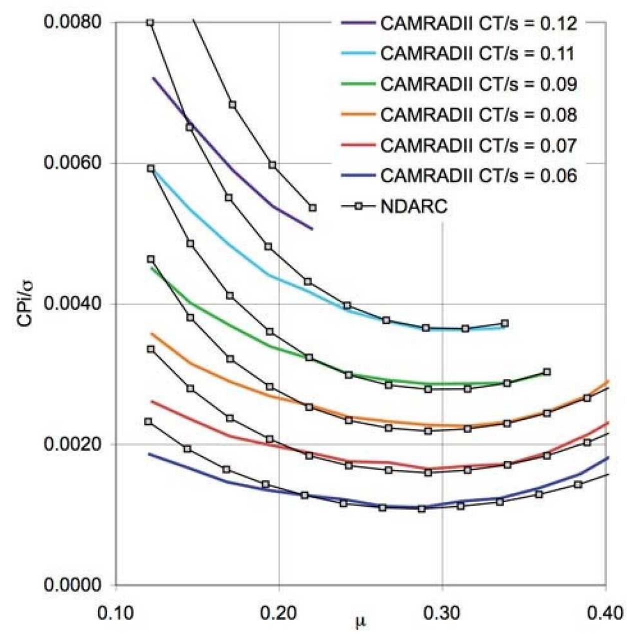

Figure 22. CH-47D rotor model: forward flight induced power for tandem rotors.

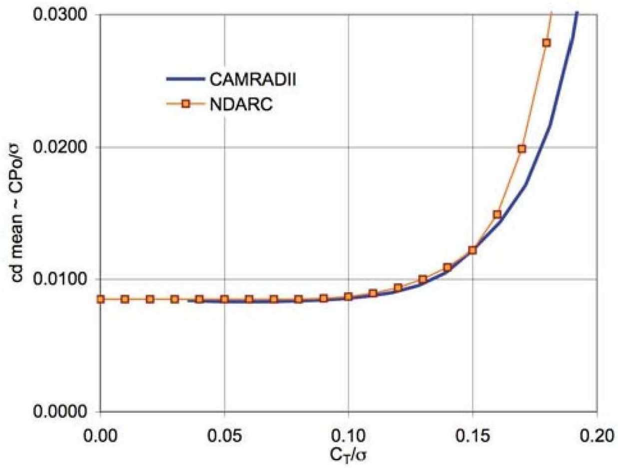

Figure 23. CH-47D rotor model: hover profile power (single rotor).

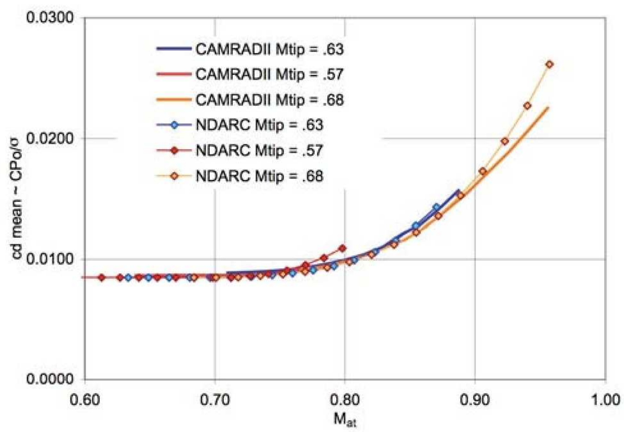

Figure 24. CH-47D rotor model: compressibility profile power (single rotor).

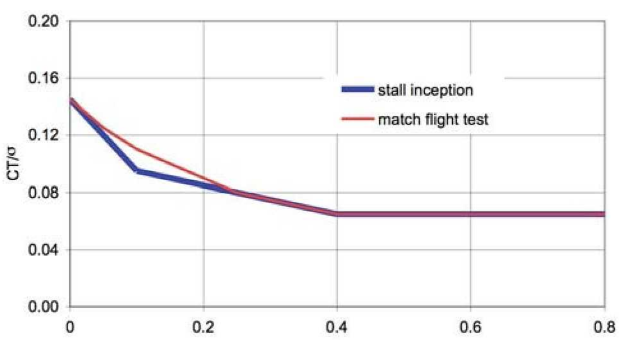

Figure 25. CH-47D rotor model: NDARC profile power stall loading $(C_T/\sigma)_s$.

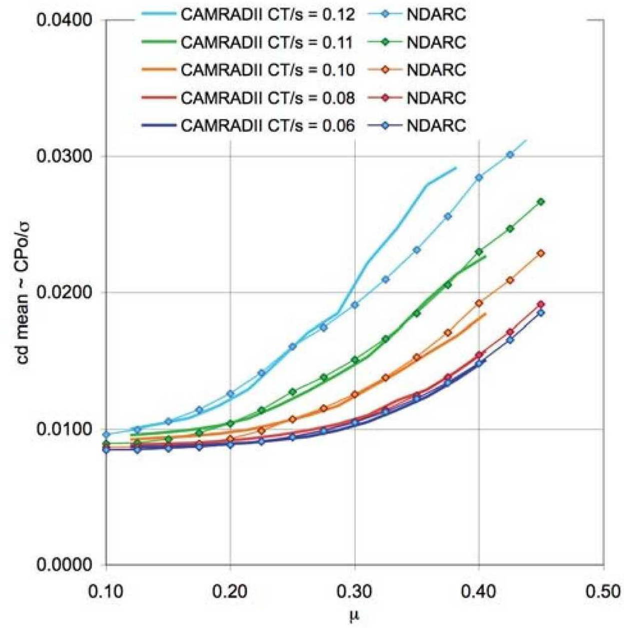

(a) NDARC parameters to match CAMRADII single rotor profile power

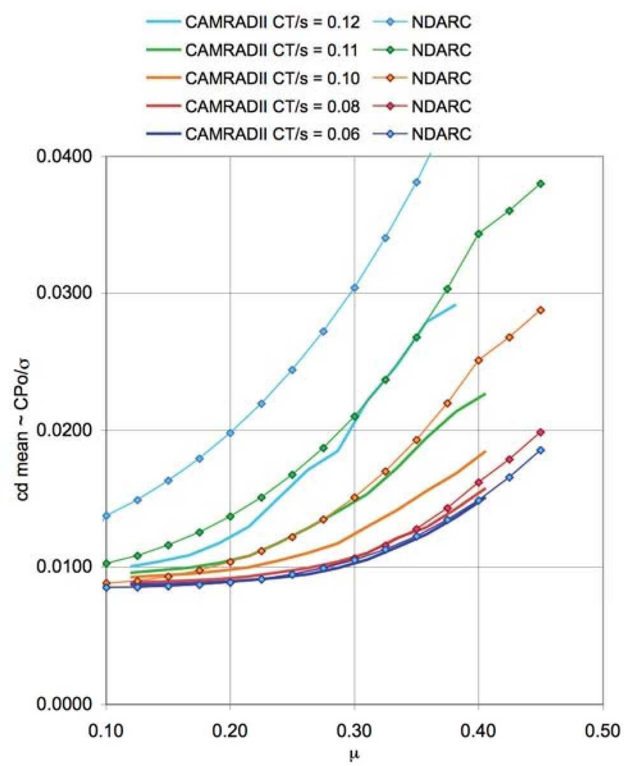

(b) NDARC parameters for better match of flight test performance at high thrust

Figure 26. CH-47D rotor Model: forward flight profile power.

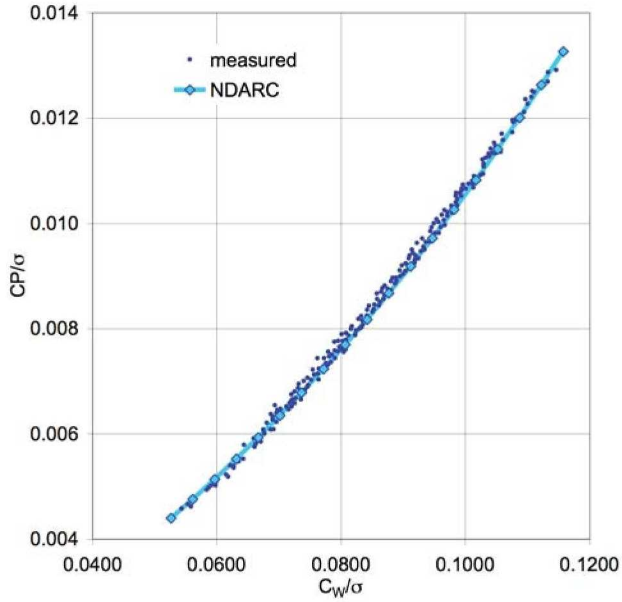

(a) rotor power

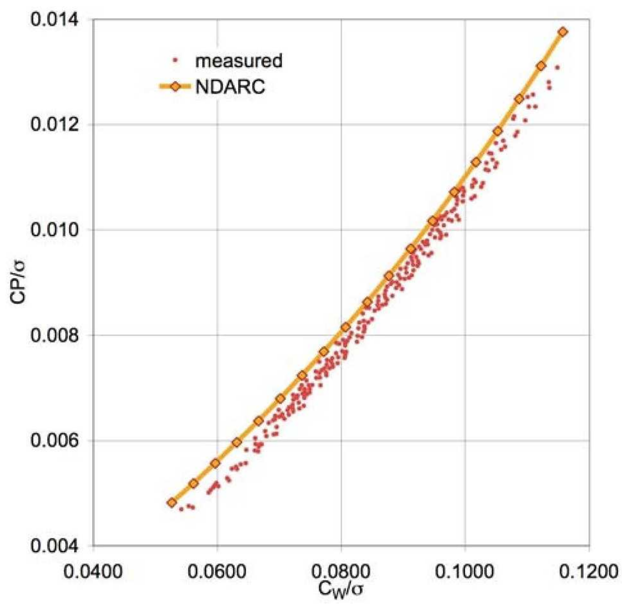

(b) aircraft power

Figure 27. Comparison of CH-47D flight test hover performance with NDARC calculations.

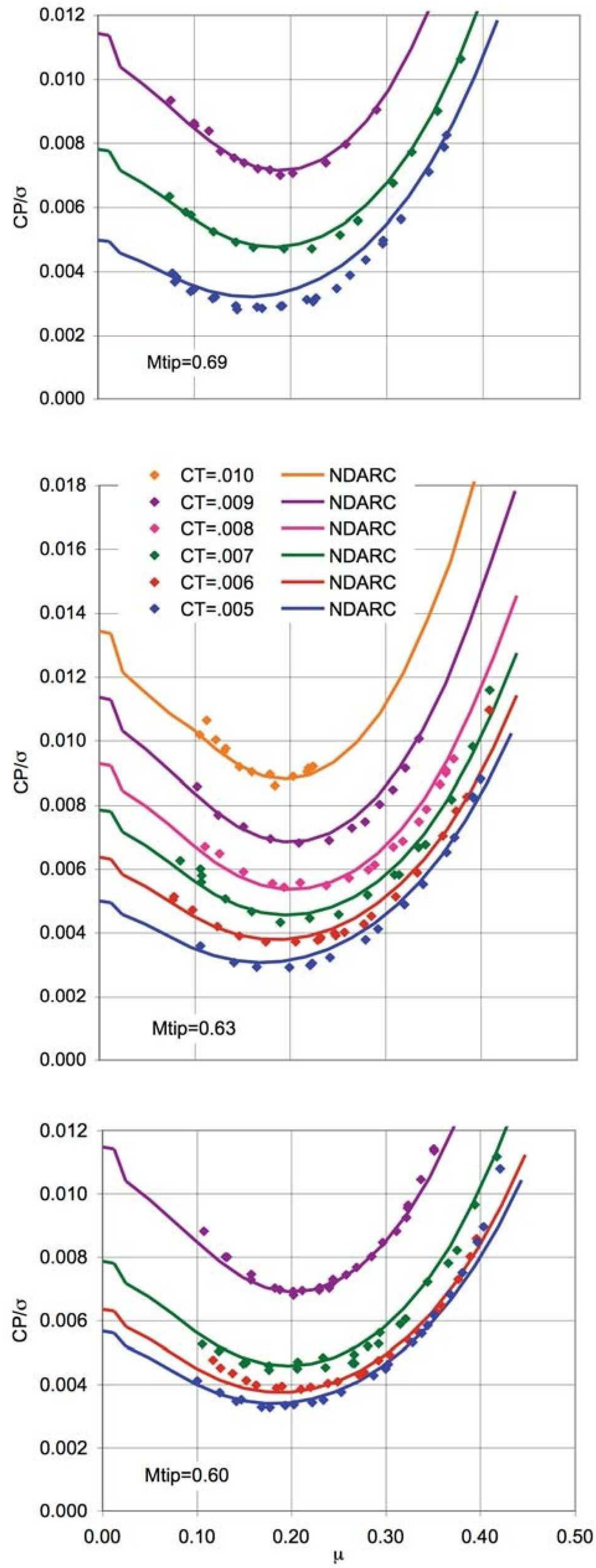

Figure 28. Comparison of CH-47D forward flight performance with NDARC calculations.

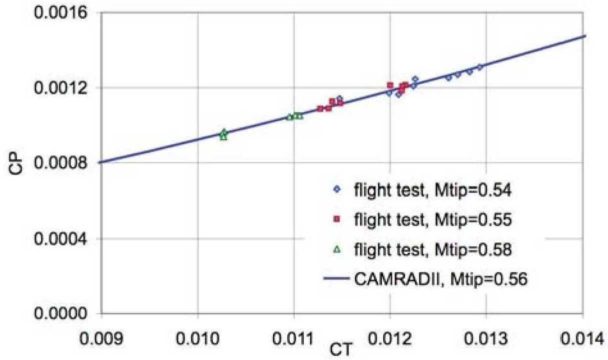

Figure 29. Comparison of XH-59A hover performance with CAMRADII calculations.

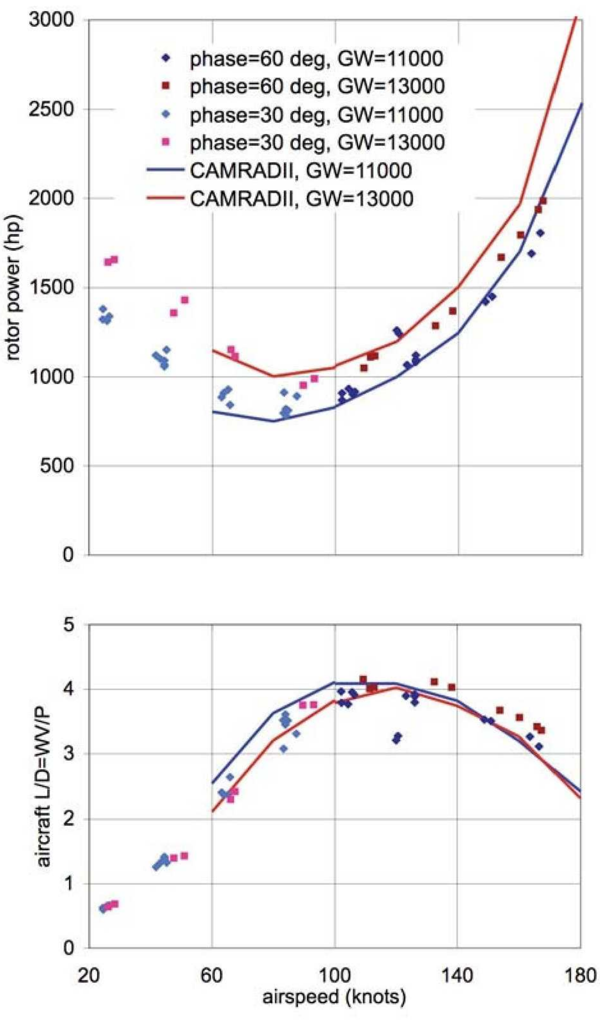

Figure 30. Comparison of XH-59A forward flight performance with CAMRADII calculations.

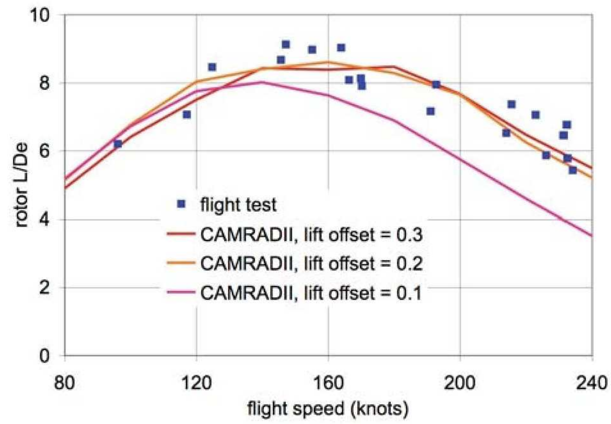

Figure 31. Comparison of XH-59A forward flight performance (using auxiliary propulsion) with CAMRADII calculations.

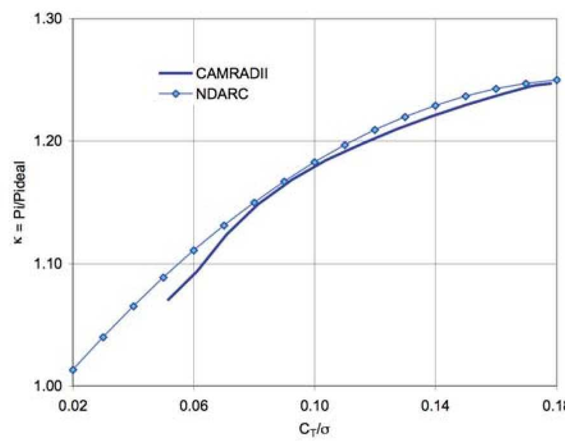

Figure 32. XH-59A rotor model: hover induced power for single rotor.

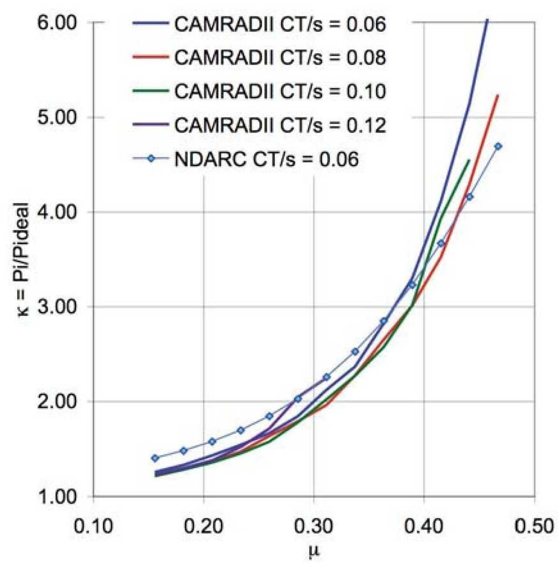

Figure 33. XH-59A rotor model: forward flight induced power for single rotor, helicopter operation.

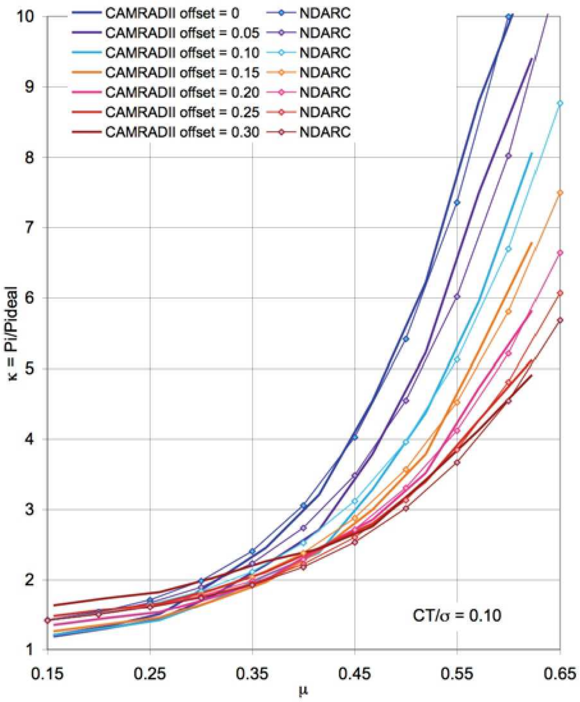

Figure 34. XH-59A rotor model: forward flight induced power for single rotor, auxiliary propulsion operation.

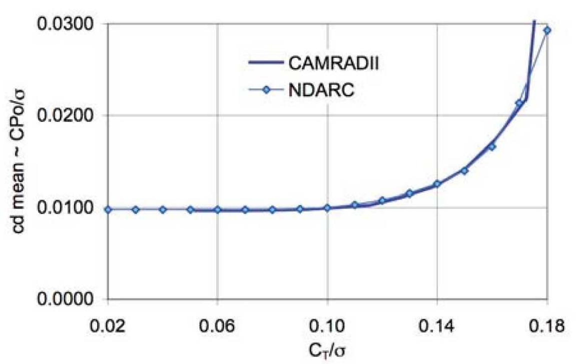

Figure 35. XH-59A rotor model: hover profile power for single rotor.

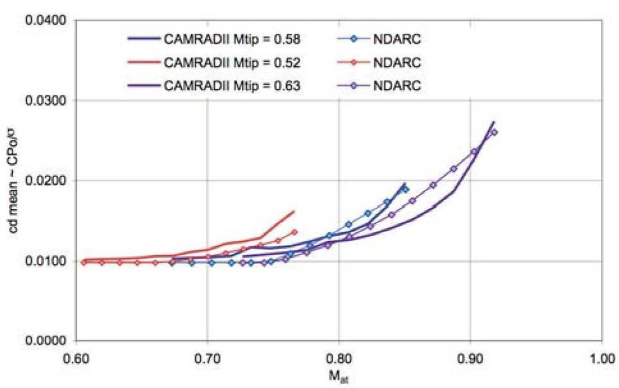

Figure 36. XH-59A rotor model: compressibility profile power for single rotor.

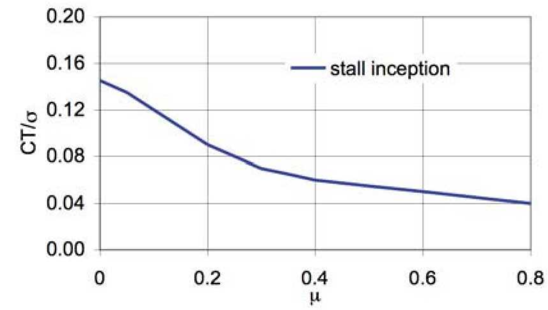

Figure 37. XH-59A rotor model: NDARC profile power stall loading $(C_T/\sigma)_s$.

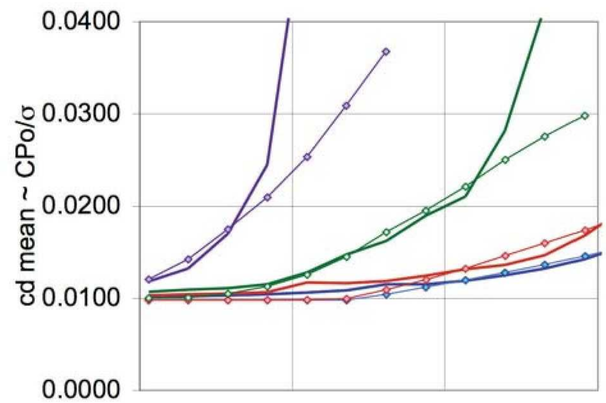

(a) NDARC parameters to match CAMRADII single rotor profile power

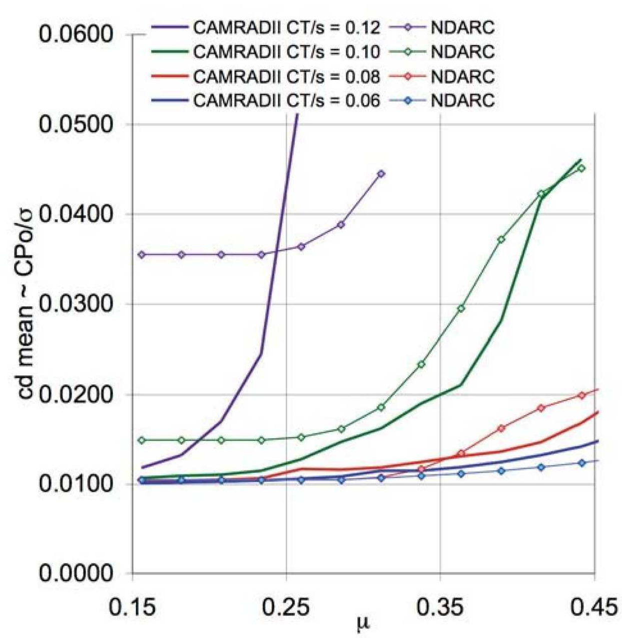

(b) NDARC parameters for better match of flight test performance

Figure 38. XH-59A rotor model: forward flight profile power, helicopter operation.

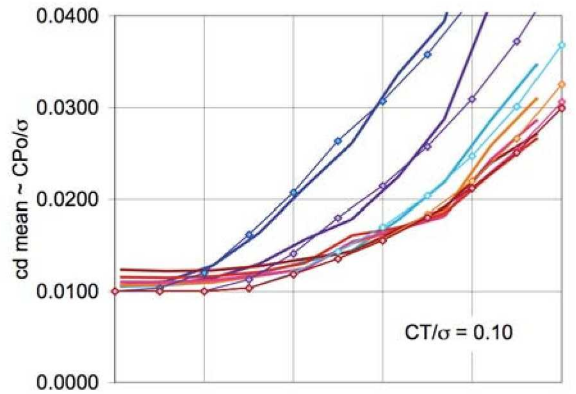

(a) NDARC parameters to match CAMRADII single rotor profile power

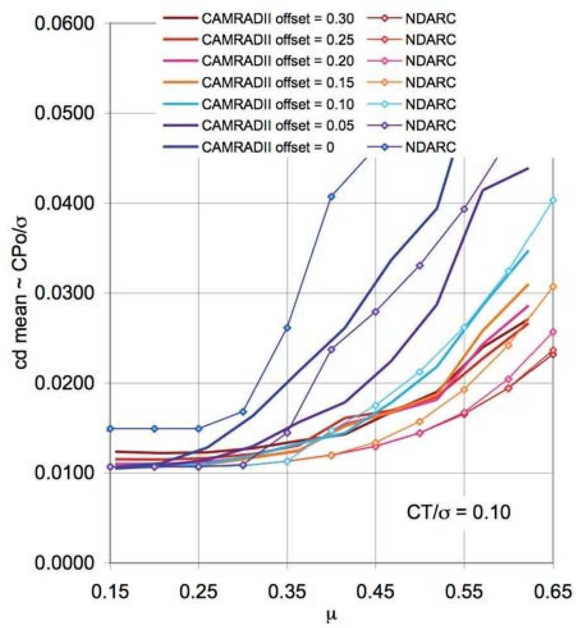

(b) NDARC parameters for better match of flight test performance

Figure 39. XH-59A rotor model: forward flight profile power, auxiliary propulsion operation.

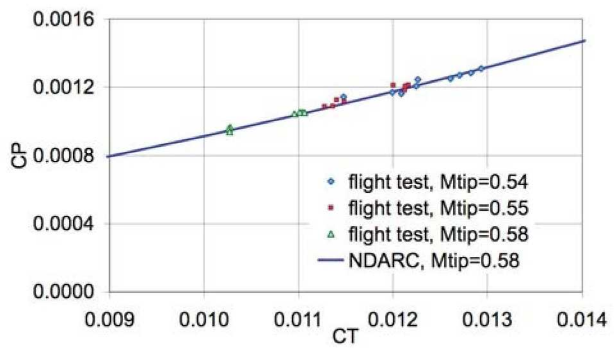

Figure 40. Comparison of XH-59A hover performance with NDARC calculations.

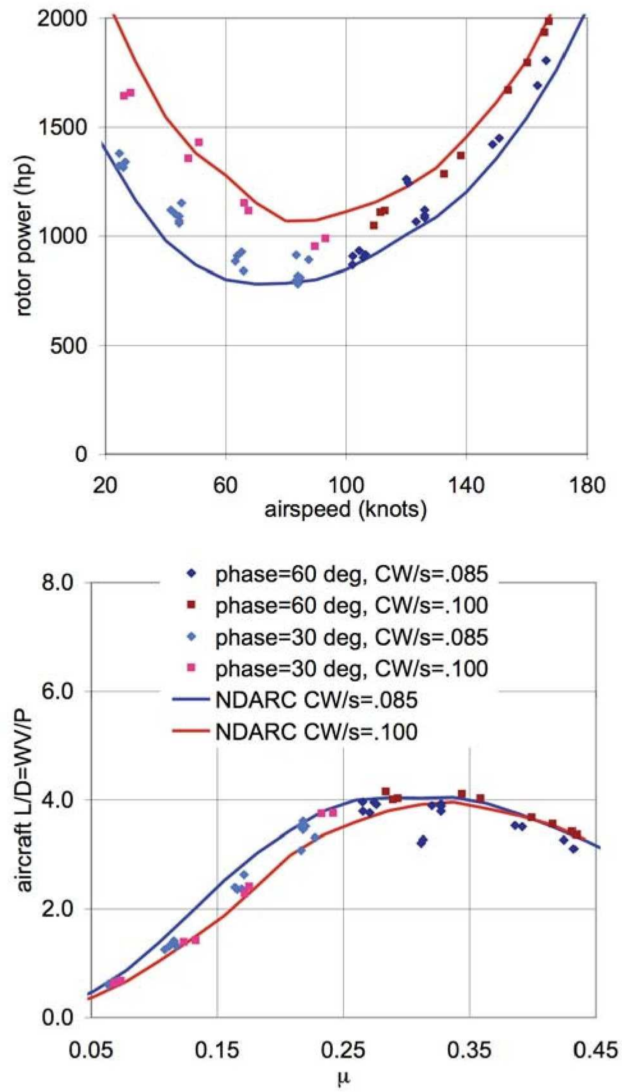

Figure 41. Comparison of XH-59A forward flight performance with NDARC calculations.

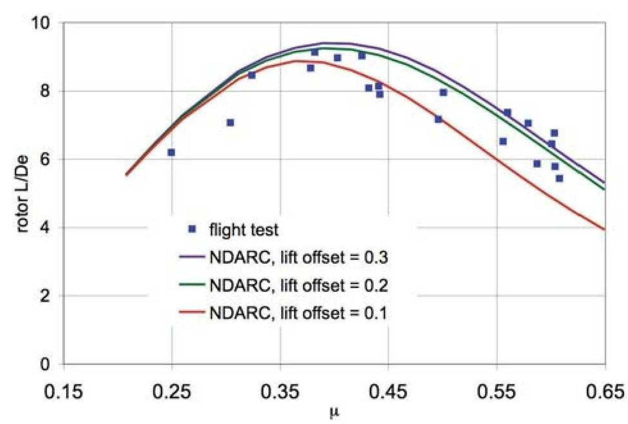

Figure 42. Comparison of XH-59A forward flight performance (using auxiliary propulsion) with NDARC calculations.

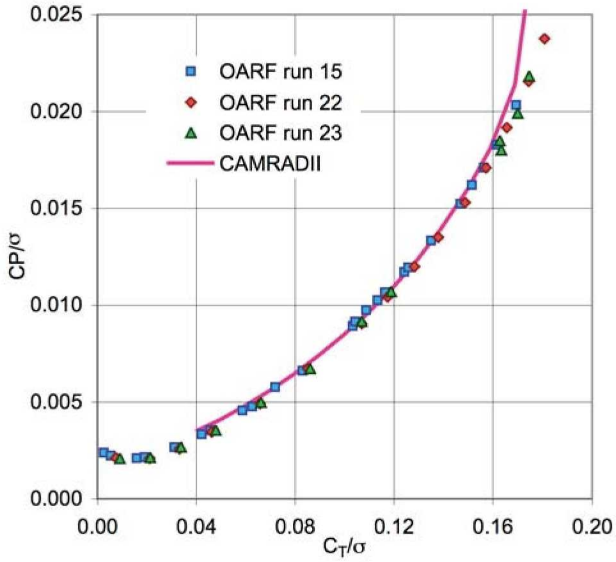

Figure 43. Comparison of XV-15 rotor hover performance with CAMRADII calculations.

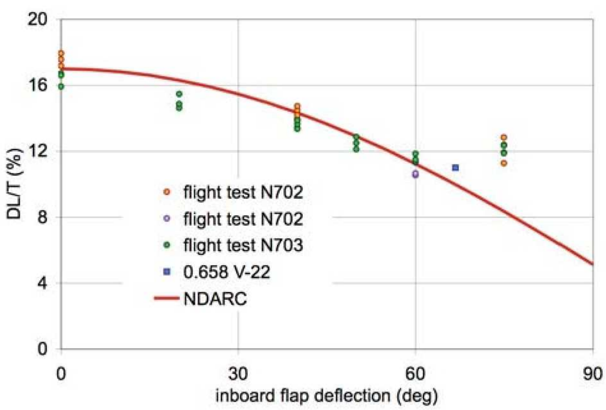

Figure 44. XV-15 hover download.

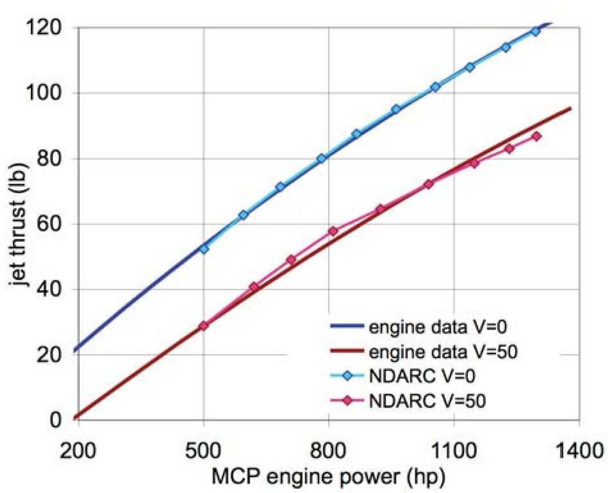

Figure 45. XV-15 engine jet thrust.

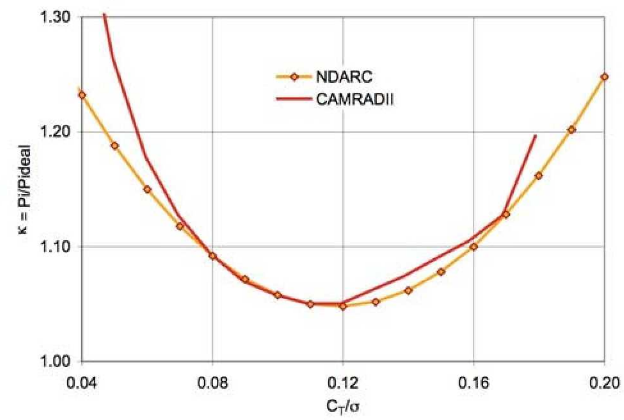

Figure 46. XV-15 rotor model: hover induced power.

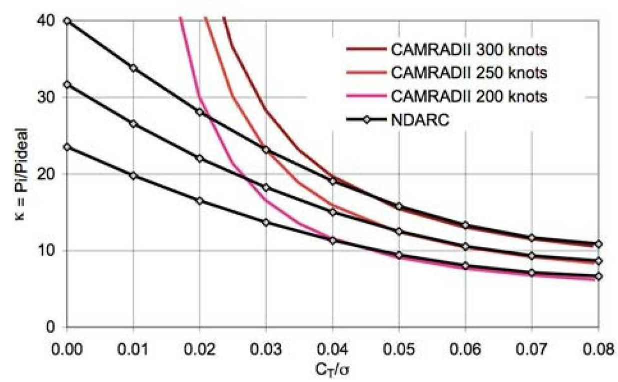

Figure 47. XV-15 rotor model: cruise induced power (axial flight).

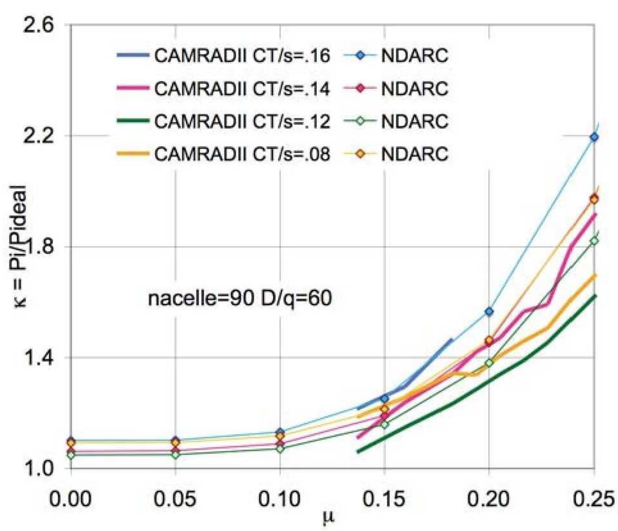

Figure 48. XV-15 rotor model: helicopter mode induced power (nacelle angle 90 deg).

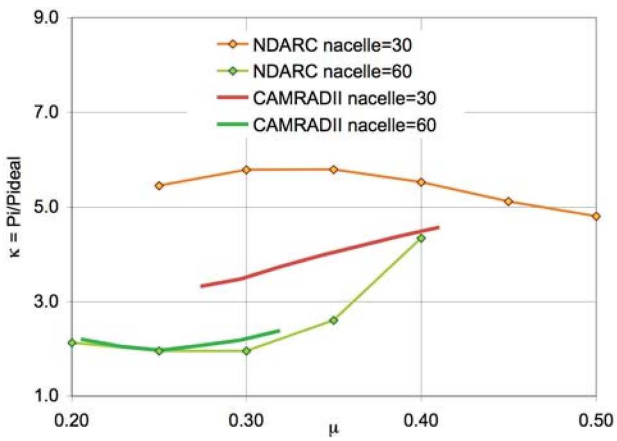

Figure 49. XV-15 rotor model: conversion mode induced power (nacelle angles 60 and 30 deg).

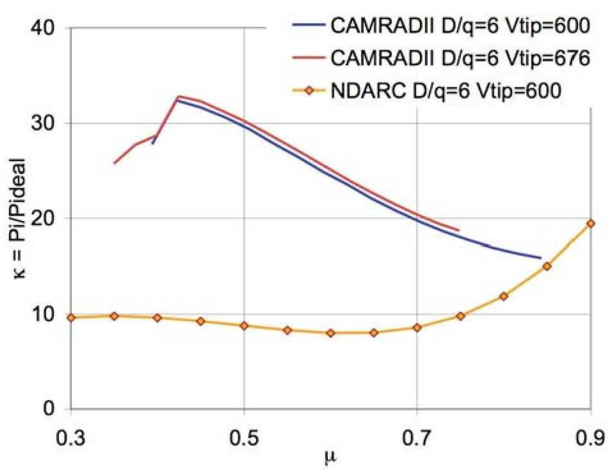

Figure 50. XV-15 rotor model: airplane mode induced power (nacelle angle 0 deg).

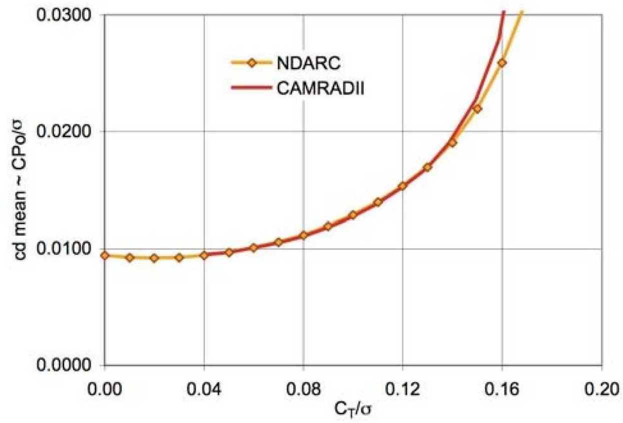

Figure 51. XV-15 rotor model: hover profile power.

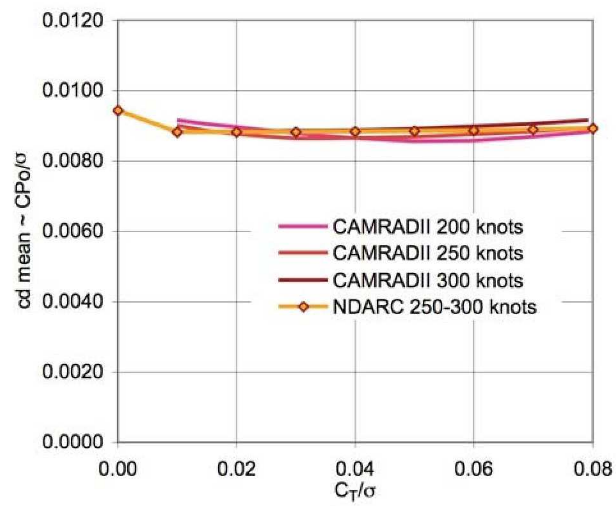

Figure 52. XV-15 rotor model: cruise profile power (axial flight).

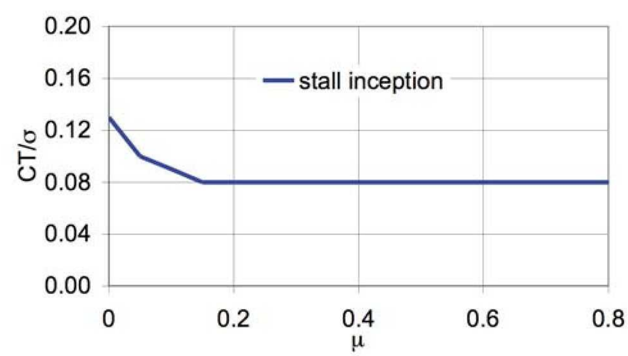

Figure 53. XV-15 rotor model: profile power stall loading $(C_T/\sigma)_s$.

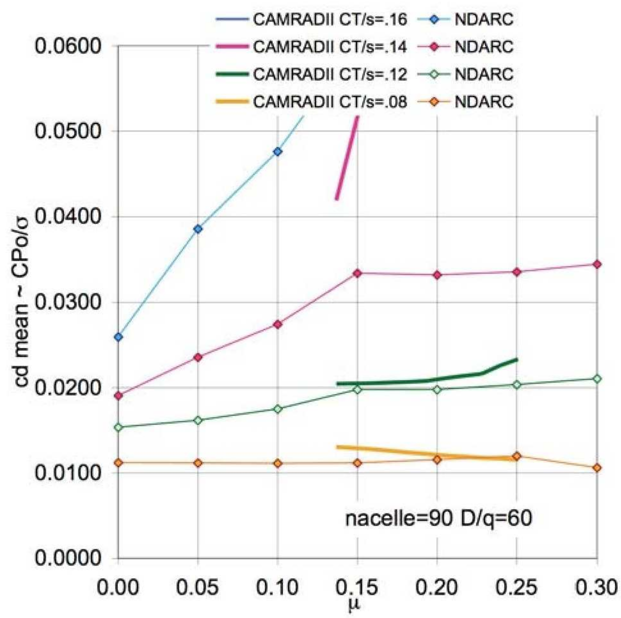

Figure 54. XV-15 rotor model: helicopter mode profile power (nacelle angle 90 deg).

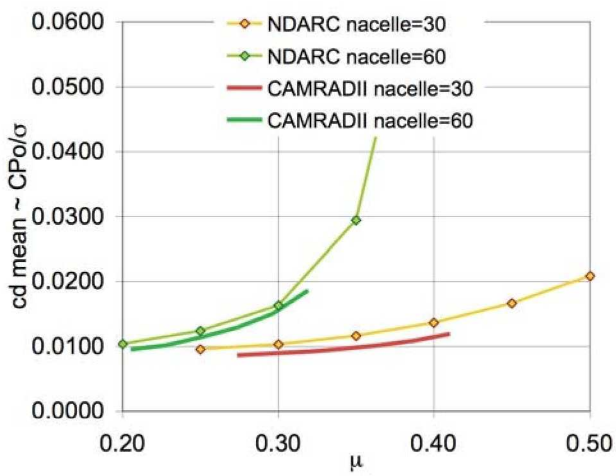

Figure 55. XV-15 rotor model: conversion mode profile power (nacelle angles 60 and 30 deg).

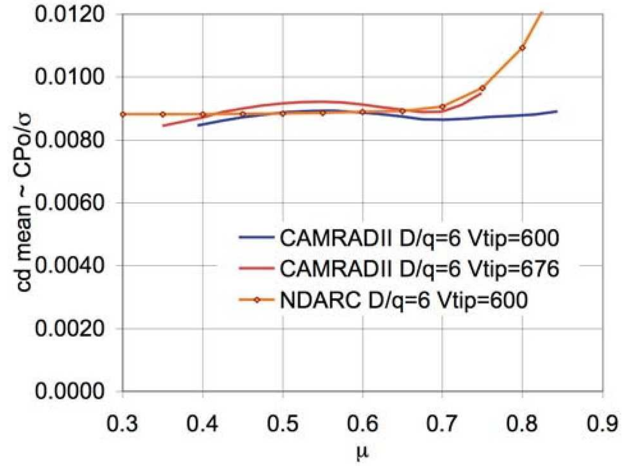

Figure 56. XV-15 rotor model: airplane mode profile power (nacelle angle 0 deg)

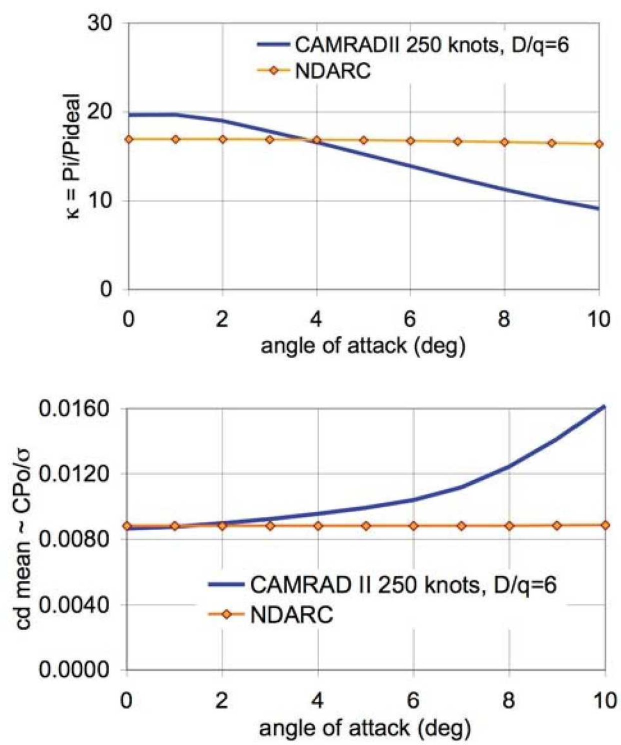

Figure 57. XV-15 rotor model: influence of shaft angle-of-attack on induced and profile power in cruise.

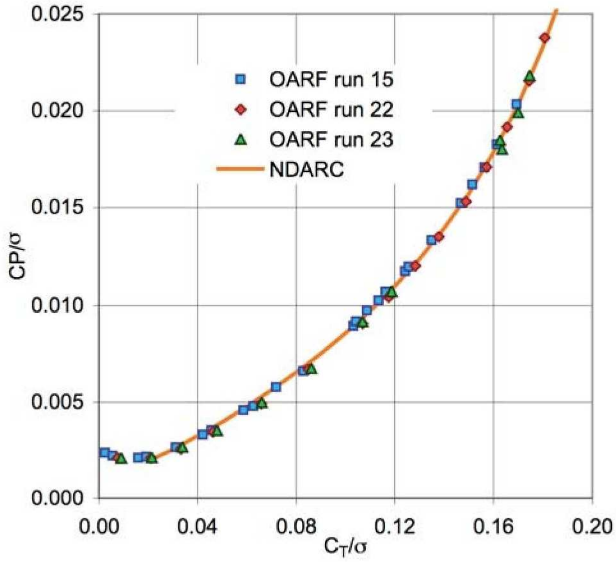

Figure 58. Comparison of XV-15 rotor hover performance with NDARC calculations.

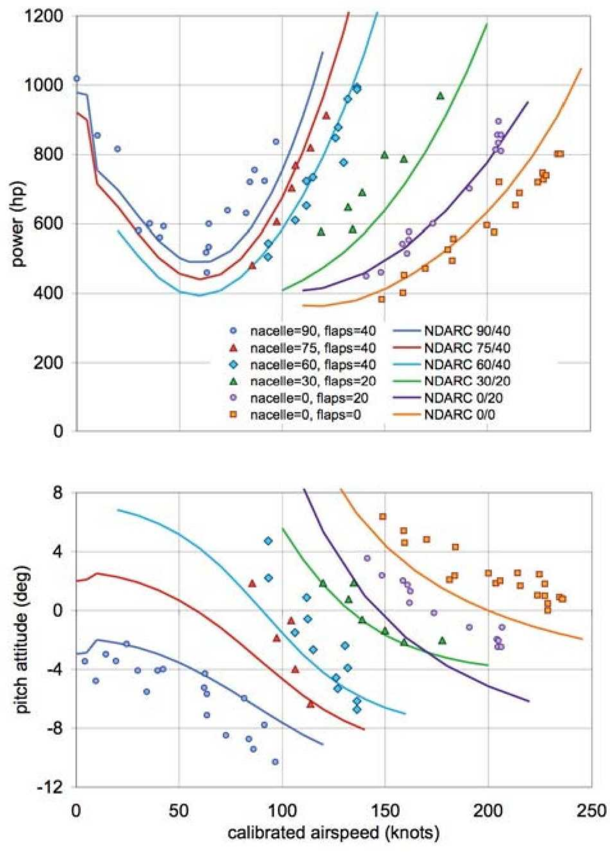

Figure 59. Comparison of XV-15 aircraft forward flight performance with NDARC calculations.

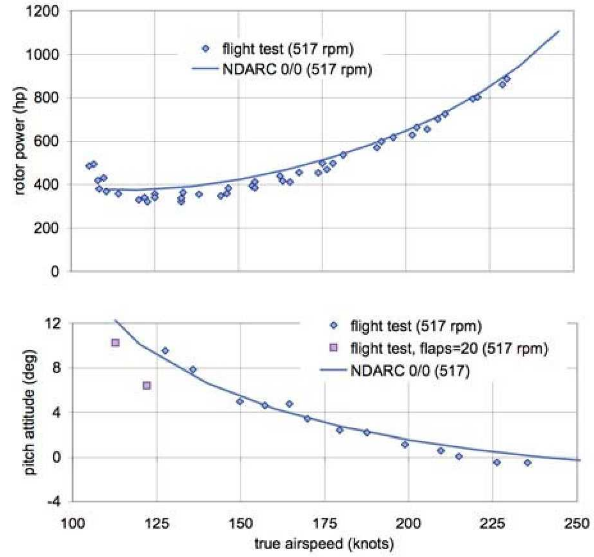

Figure 60. Comparison of XV-15 aircraft forward flight performance with NDARC calculations.

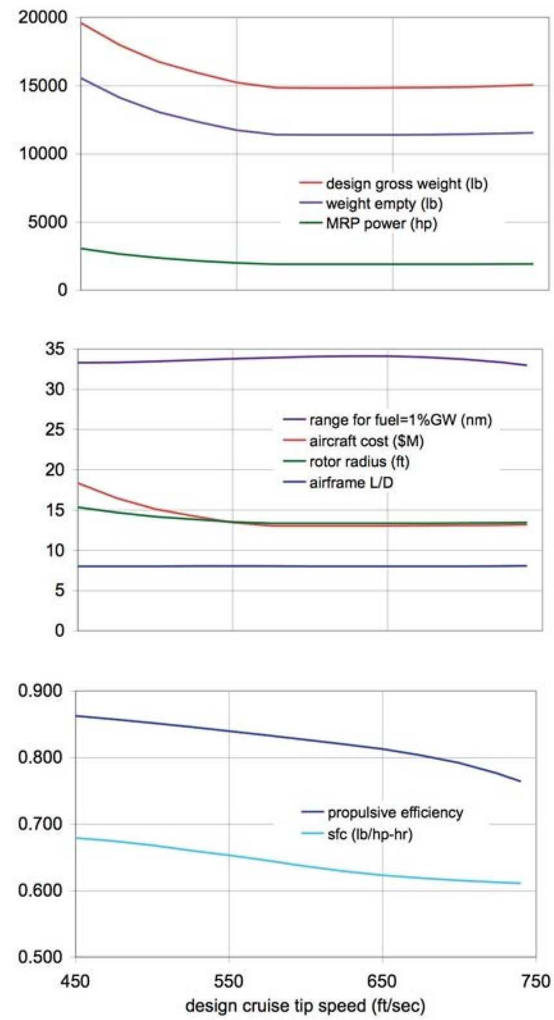

Figure 61. Influence of design cruise tip speed on tiltrotor size and efficiency.